ELSEVIER

European Journal of Mechanics B/Fluids 21 (2002) 447–468

EUROPEAN JOURNAL OF MECHANICS B/FLUIDS

Unsteady heat transfer in impulsive Falkner–Skan flows: Constant wall temperature case

Simon D. Harris [a], Derek B. Ingham [b], Ioan Pop [c,*]

[a] *Rock Deformation Research, School of Earth Sciences, University of Leeds, Leeds LS2 9JT, UK*
[b] *Department of Applied Mathematics, University of Leeds, Leeds LS2 9JT, UK*
[c] *Faculty of Mathematics, University of Cluj, R–3400 Cluj, CP 253, Romania*

Received 11 September 2001; received in revised form 19 March 2002; accepted 11 April 2002

Abstract

A theoretical study of the velocity and thermal boundary-layer growth resulting from an impulsively started Falkner–Skan flow is presented in this paper. The forced convection, thermal boundary-layer is produced by the sudden increase of the surface temperature as it is set into motion. Analytical solutions for the simultaneous development of the thermal and momentum boundary layers are obtained for both small (initial, unsteady flow) and large (steady-state flow) times. These solutions are then matched numerically using a very efficient finite-difference scheme. Some considerable attention to the steady-state flow solution (large time) is also given in this paper. Results of the calculations are presented for a range of values of the Falkner–Skan exponent m and the Prandtl number Pr.

Keywords: Falkner–Skan; Semi-infinite wedge; Isothermal; Transient flow; Steady-state flow; Boundary-layer; Analytical and numerical solutions

1. Introduction

The steady Falkner–Skan problem is a classical one and has been studied by many investigators, see, for example, Leal [1], Gersten and Herwig [2], and Schlichting and Gersten [3]. In recent years, unsteady conditions of motion and heating of bodies in fluids have been increasingly important in certain applications within some engineering fields of aerodynamics and hydrodynamics. For example, standard types of aerodynamic experiments have been performed in shock tunnels for a number of years, but test times are generally so short that solid surfaces are not able to heat up to temperatures simulating actual conditions. Lacking a description of the transient development process, it has not been possible to design model configurations where these limitations might be overcome.

There is a large body of literature on unsteady, forced convection, boundary-layer flows past bodies of different geometries which give rise to the Falkner–Skan equations, see Riley [4,5], Telionis [6,7], and Ludlow et al. [8]. However, fewer studies have been concerned with the heat transfer aspects, see Pop [9]. When the fluid is assumed to have constant properties, then the problem reduces to an uncoupled, laminar, boundary-layer flow and the fluid velocity field is unaffected by any temperature changes. However, the problem becomes coupled when the thermophysical fluid properties depend on the temperature, so that the fluid velocity is also a function of time. The unsteady flow has direct relevance to the oscillation cycle of pitching aerofoils,

* Correspondence and reprints.
E-mail address: popi@math.ubbcluj.ro (I. Pop).

0997-7546/02/$ – see front matter
PII: S0997-7546(02)01193-7

Nomenclature

C_f	skin friction coefficient
f	non-dimensional, reduced stream function
f_∞	large time, steady-state solution for f
F	non-dimensional stream function f expressed in terms of ζ
$\mathcal{F}$	non-dimensional fluid velocity function
g	non-dimensional, reduced temperature function
g_∞	large time, steady-state solution for g
G	non-dimensional temperature function g expressed in terms of ζ
k_f	thermal conductivity of the fluid
l	characteristic length
m	exponent
m^*	value of m at which the boundary-layer breaks down
Nu	Nusselt number
Pr	Prandtl number
$q_w(\bar{x})$	variable surface heat flux
Re	Reynolds number
Re_x	local Reynolds number
$\bar{t}$	time
$\overline{T}$	fluid temperature
T_w	surface temperature of the wedge
T_∞	ambient temperature
$\bar{u}_e(\bar{x})$	velocity of the potential flow
U_∞	constant speed of the wedge along its plane of symmetry
$\bar{u}$, $\bar{v}$	velocity components along the $\bar{x}$- and $\bar{y}$-axes, respectively
$\bar{x}$, $\bar{y}$	Cartesian coordinates measured along the surface of the wedge and normal to it, respectively
Greek symbols	
β	constant defining the included angle $\pi\beta$ of the wedge
ρ	fluid density
ζ, η	transformed spatial variables
μ	dynamic viscosity
ν	kinematic viscosity
τ	non-dimensional, reduced time
$\tau_w(\bar{x})$	skin friction along the wedge surface
Φ	non-dimensional fluid velocity function
ψ	non-dimensional stream function

such as those of helicopter rotors, where the heat transfer results are relevant to the determination of the surface heat flux and the subsequent temperature variations in the blade.

The situation considered in this paper is that of heat transfer in the unsteady, thermal boundary-layer associated with the forced convection (momentum) boundary-layer flow resulting from a transient Falkner–Skan problem with exponent m. This situation has physical relevance when $0 < m \leqslant 1$ and, for such cases, the flow is that of an incompressible fluid past a sharp, semi-infinite wedge of included angle $2m\pi/(m+1)$. The surface is set impulsively into motion at (non-dimensional) time $t = 0$ and this gives rise to a non-dimensional potential flow with $u_e(x) = x^m$, where x is the non-dimensional distance along the surface from the leading edge and $u_e(x)$ is the x component of the potential velocity on the surface. The surface and the fluid are initially at the same temperature T_∞. In addition, at $t = 0$, the thermal boundary-layer is produced by the simultaneous sudden imposition of a constant temperature T_w ($> T_\infty$) over the surface. Constant boundary-layer properties are assumed and viscous dissipation effects are neglected. This problem has wide applications and is related to the flow created by the passage of a shock wave over a surface, see Walker and Dennis [10].

The study of the unsteady, incompressible, forced convection, boundary-layer flow past a semi-infinite wedge impulsively set into motion was initiated by Smith [11], and this problem was subsequently solved numerically by Nanbu [12] using the method proposed by Hall [13]. This method solves the untransformed equations directly using an iterative procedure and a finite-difference technique for unsteady boundary layers. Watkins [14] has also solved this problem numerically following a second

order, zig–zag, finite-difference scheme devised by Krause, see Krause and Bothmann [15]. This scheme has the feature of utilising downstream information at an earlier time in the development of the flow, as well as current upstream information, to predict the properties of a boundary-layer containing a local flow reversal. Watkins [14] has also studied the unsteady heat transfer aspects of the semi-infinite wedge started impulsively from rest to include solutions of the energy equation. A new set of scaled coordinates, introduced by Williams and Rhyne [16], for investigating the development of the forced convection, boundary-layer flow past a wedge impulsively set into motion were used. It was found that the flow is affected by the leading edge, and the effect is in the direction of increasing x for $t > x/(1-m)u_e$ ($m < 1$). This change in character of the flow manifests itself mathematically as a change in character of the equations which describe the transition of the boundary-layer from the initial Rayleigh solution to the final, steady-state Falkner–Skan solution. Tsay and Shih [17] used a perturbation method to study the steady and unsteady, laminar boundary-layer heat transfer from a wedge of angle $\pi\beta/2$ with separation ($\beta = -0.198838$) for large or moderate values of the Prandtl number.

The numerical calculation of unsteady boundary layers is of considerable interest at the present time, partly as an approach to the resolution of difficult features of steady boundary layers, partly because of its importance in certain problems of practical interest (for example in aerodynamics), and partly for its own sake. The present paper is concerned with Watkins' [14] heat transfer problem for an impulsively started Falkner–Skan flow, and the majority of cases considered relate to the acute, semi-infinite wedge problem. The initial development of the thermal boundary-layer has satisfactorily been represented by a series solution for small times. Physically, at this initial stage of the transient process, diffusion dominates convection, which is affected only weakly by the velocity components close to the surface. The solution for large time approaches steady state and is given by the Falkner–Skan equation. The results obtained for the heat transfer characteristics during the initial and final stages of the motion are supplemented by a numerical integration of the transformed boundary-layer equations. The very detailed numerical solution is presented for the whole transient from the initial ($\tau = 0$) unsteady to the final ($\tau \to \infty$) steady state by using a modification of the step-by-step method proposed by Merkin [18], in combination with a finite-difference method similar to that devised by Dennis [19], approaches which have been very successfully used recently on a range of problems by Harris et al. [20–24].

2. Basic equations

The generalized impulsive Falkner–Skan system that we consider is based upon the problem of the unsteady, two-dimensional, viscous flow of an incompressible fluid past a symmetrical, sharp wedge with an $\bar{x}$ and $\bar{y}$ coordinate system, where $\bar{x}$ is measured along the surface of the wedge from the apex and $\bar{y}$ is measured normal to the surface, see Fig. 1. At time $\bar{t} = 0$, the wedge is impulsively set into motion with a uniform speed U_∞ along its plane of symmetry in an otherwise stationary, viscous and incompressible fluid. The heat transfer problem is idealised as follows. The wedge and the fluid are assumed to be initially at the same temperature T_∞. A thermal boundary-layer is then produced by the sudden increase of the temperature of the wedge to a constant value T_w ($> T_\infty$) as the wedge is set into motion. The inviscid flow over the wedge develops instantaneously and its velocity is given by

$$\bar{u}_e(\bar{x}) = U_\infty \left(\frac{\bar{x}}{l}\right)^m \quad \text{for } m \leqslant 1, \tag{1}$$

where l is a characteristic length and m is related to the included angle $\pi\beta$ by $m = \beta/(2-\beta)$. It is clear that for negative values of m the solution becomes singular at $\bar{x} = 0$, whilst for m positive the solution can be defined for all values of $\bar{x}$, and this leads

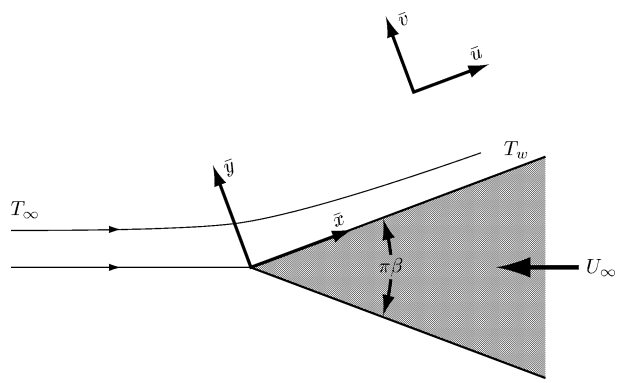

Fig. 1. Physical model and coordinate system.

to a general difference between the solutions for the cases of $m < 0$ and $m \geqslant 0$. The particular cases of Blasius' solution for a flat plate ($\beta = 0$, $m = 0$), stagnation point flow ($\beta = 1$, $m = 1$), together with the wedge angles 30° ($\beta = 1/6$, $m = 1/11$), 60° ($\beta = 1/3$, $m = 1/5$), and 90° ($\beta = 1/2$, $m = 1/3$), will be considered for different values of the Prandtl number Pr. We will also consider in more detail the steady flow case ($\tau \to \infty$), described by the Falkner–Skan equation, for two values of the parameter m, namely $m = 0$ ($\beta = 0$) and $m = 2$ ($\beta = 4/3$), which corresponds to a wedge angle of 240°. However, for physical applications we require that $0 < \beta \leqslant 1$, since the acute wedge angle is $\pi\beta$, and this upper limit corresponds to $m = 1$. Other values of m will be considered within the Blasius-like solution range $m^* \leqslant m < \infty$, where m^* is the minimum value of m for which boundary-layer separation occurs. When $m^* \leqslant m < 0$ and $m > 1$, the situation is no longer physically relevant with respect to the acute, semi-infinite wedge problem. However, such cases are of considerable mathematical interest and have intrigued the applied mathematics community for many years.

We introduce non-dimensional variables according to

$$x = \frac{\bar{x}}{l}, \qquad y = \mathrm{Re}^{\frac{1}{2}}\frac{\bar{y}}{l}, \qquad u = \frac{\bar{u}}{U_\infty}, \qquad v = \mathrm{Re}^{\frac{1}{2}}\frac{\bar{v}}{U_\infty}, \qquad u_e = \frac{\bar{u}_e}{U_\infty}, \qquad t = \frac{U_\infty}{l}\bar{t}, \qquad T = \frac{\overline{T} - T_\infty}{T_w - T_\infty}, \tag{2}$$

where $\mathrm{Re} = U_\infty(l/\nu)$ is the Reynolds number, $\bar{u}$ and $\bar{v}$ are the velocity components along the $\bar{x}$- and $\bar{y}$-axes, respectively, $\overline{T}$ is the fluid temperature, and ν is the kinematic viscosity. The velocity over the wedge is now given by

$$u_e(x) = x^m \quad \text{for } m \leqslant 1 \tag{3}$$

and, sufficiently far downstream from the apex, the governing equations can be written as

$$\frac{\partial u}{\partial x} + \frac{\partial v}{\partial y} = 0, \tag{4}$$

$$\frac{\partial u}{\partial t} + u\frac{\partial u}{\partial x} + v\frac{\partial u}{\partial y} = u_e\frac{\partial u_e}{\partial x} + \frac{\partial^2 u}{\partial y^2}, \tag{5}$$

$$\frac{\partial T}{\partial t} + u\frac{\partial T}{\partial x} + v\frac{\partial T}{\partial y} = \frac{1}{Pr}\frac{\partial^2 T}{\partial y^2}, \tag{6}$$

which must be solved subject to the initial and boundary conditions

$$\left.\begin{array}{llll} u = 0, & v = 0, & T = 0 & \text{for all } x, y \\ u = 0, & v = 0, & T = 1 & \text{on } y = 0,\ x > 0 \\ u \to u_e(x), & & T \to 0 & \text{as } y \to \infty,\ x > 0 \end{array}\right\} \quad \begin{array}{l} \text{for } t < 0, \\ \\ \text{for } t \geqslant 0. \end{array} \tag{7}$$

The number of independent variables in the governing equations can be reduced from three to two by introducing the non-dimensional, reduced stream function $f(\eta, \tau)$ and the non-dimensional, reduced temperature function $g(\eta, \tau)$ according to

$$\psi = x^{\frac{m+1}{2}} f(\eta, \tau), \qquad T = g(\eta, \tau), \qquad \eta = x^{\frac{m-1}{2}} y, \qquad \tau = x^{m-1} t, \tag{8}$$

where η is a non-dimensional similarity variable and ψ is the stream function, which is defined in the usual way, namely $u = \partial\psi/\partial y$ and $v = -\partial\psi/\partial x$. Substituting the transformation (8) into Eqs. (5) and (6), we obtain

$$\frac{\partial^3 f}{\partial \eta^3} + \left[\frac{m+1}{2} f + (m-1)\tau\frac{\partial f}{\partial \tau}\right]\frac{\partial^2 f}{\partial \eta^2} + m\left[1 - \left(\frac{\partial f}{\partial \eta}\right)^2\right] = \left[1 + \left(m - 1\right)\tau\frac{\partial f}{\partial \eta}\right]\frac{\partial^2 f}{\partial \eta \partial \tau}, \tag{9}$$

$$\frac{1}{\mathrm{Pr}}\frac{\partial^2 g}{\partial \eta^2} + \left[\frac{m+1}{2} f + (m-1)\tau\frac{\partial f}{\partial \tau}\right]\frac{\partial g}{\partial \eta} = \left[1 + (m-1)\tau\frac{\partial f}{\partial \eta}\right]\frac{\partial g}{\partial \tau}, \tag{10}$$

and the boundary conditions (7) become

$$f(0, \tau) = 0, \qquad \frac{\partial f}{\partial \eta}(0, \tau) = 0, \qquad g(0, \tau) = 1, \qquad \frac{\partial f}{\partial \eta}(\eta, \tau) \to 1, \quad g(\eta, \tau) \to 0 \quad \text{as } \eta \to \infty, \tag{11}$$

for $\tau \geqslant 0$.

3. Small time solution, $\tau \ll 1$

Eqs. (9) and (10) must now be written in a form which is much more convenient for analysis at small times. In all impulsive changes in temperature or heat flux problems there is a short period during which the effects are confined to a thin,

one-dimensional boundary-layer which is adjacent to the surface. Since the appropriate length scale for small times is the diffusion scale $\tau^{1/2}$, we introduce the following variables:

$$f = 2\tau^{\frac{1}{2}} F(\zeta,\tau), \qquad g = G(\zeta,\tau), \qquad \zeta = \frac{\eta}{2\tau^{1/2}}. \tag{12}$$

Substituting these variables into Eqs. (9) and (10) yields

$$\frac{\partial^3 F}{\partial\zeta^3} + \left[2\zeta + 4m\tau F + 4(m-1)\tau^2\frac{\partial F}{\partial\tau}\right]\frac{\partial^2 F}{\partial\zeta^2} + 4m\tau\left[1-\left(\frac{\partial F}{\partial\zeta}\right)^2\right] = 4\tau\left[1+(m-1)\tau\frac{\partial F}{\partial\zeta}\right]\frac{\partial^2 F}{\partial\zeta\,\partial\tau}, \tag{13}$$

$$\frac{1}{\mathrm{Pr}}\frac{\partial^2 G}{\partial\zeta^2} + \left[2\zeta + 4m\tau F + 4(m-1)\tau^2\frac{\partial F}{\partial\tau}\right]\frac{\partial G}{\partial\zeta} = 4\tau\left[1+(m-1)\tau\frac{\partial F}{\partial\zeta}\right]\frac{\partial G}{\partial\tau}, \tag{14}$$

and the corresponding boundary conditions (11) become

$$F(0,\tau)=0, \qquad \frac{\partial F}{\partial\zeta}(0,\tau)=0, \qquad G(0,\tau)=1, \qquad \frac{\partial F}{\partial\zeta}(\zeta,\tau)\to 1, \quad G(\zeta,\tau)\to 0 \quad \text{as } \zeta\to\infty. \tag{15}$$

It can easily be verified that the solutions of Eqs. (13) and (14) at small values of τ ($\ll 1$) have the following form:

$$F(\zeta,\tau) = F_0(\zeta) + F_1(\zeta)\tau + F_2(\zeta)\tau^2 + \cdots, \qquad G(\zeta,\tau) = G_0(\zeta) + G_1(\zeta)\tau + G_2(\zeta)\tau^2 + \cdots. \tag{16}$$

The solutions for F_i and G_i, for $i = 0, 1, 2, \ldots$, are determined by substituting these general forms for $F(\zeta,\tau)$ and $G(\zeta,\tau)$ into Eqs. (13) and (14) and equating coefficients of powers of τ. The first two resulting systems of ordinary differential equations are as follows:

$$\begin{aligned} &F_0''' + 2\zeta F_0'' = 0, \qquad \frac{1}{\mathrm{Pr}}G_0'' + 2\zeta G_0' = 0,\\ &F_0(0)=0, \qquad F_0'(0)=0, \qquad G_0(0)=1, \qquad F_0'(\zeta)\to 1, \quad G_0(\zeta)\to 0 \quad \text{as } \zeta\to\infty, \end{aligned} \tag{17}$$

$$\begin{aligned} &F_1''' + 2\zeta F_1'' - 4F_1' = -4m\big(1 - F_0'^2 + F_0F_0''\big), \qquad \frac{1}{\mathrm{Pr}}G_1'' + 2\zeta G_1' - 4G_1 = -4mF_0G_0',\\ &F_1(0)=0, \qquad F_1'(0)=0, \qquad G_1(0)=0, \qquad F_1'(\zeta)\to 0, \quad G_1(\zeta)\to 0 \quad \text{as } \zeta\to\infty, \end{aligned} \tag{18}$$

where primes denote differentiation with respect to ζ.

The solutions of the systems (17) and (18) are as follows:

$$\begin{aligned} F_0(\zeta) &= \zeta\,\mathrm{erf}\,\zeta + \frac{1}{\sqrt{\pi}}\big(\mathrm{e}^{-\zeta^2}-1\big), \qquad G_0(\zeta) = \mathrm{erfc}\big(\sqrt{\mathrm{Pr}}\,\zeta\big),\\ F_1(\zeta) &= m\zeta\left(\frac{1}{2}-\frac{1}{3}\zeta^2\right)\mathrm{erf}\,\zeta\,\mathrm{erfc}\,\zeta + m\left[\frac{1}{\sqrt{\pi}}\left(\frac{11}{6}-\frac{2}{3}\zeta^2\right)\mathrm{e}^{-\zeta^2} + \frac{2}{3\sqrt{\pi}} - \frac{2}{3\pi}\zeta - \left(\frac{2}{3}+\frac{4}{9\pi}\right)\zeta^3\right]\mathrm{erfc}\,\zeta\\ &\quad + m\left\{\frac{1}{3\pi}\zeta\,\mathrm{e}^{-\zeta^2} + \frac{1}{\sqrt{\pi}}\left[-\frac{3}{2}+\frac{4}{9\pi}+\left(1+\frac{4}{9\pi}\right)\zeta^2\right]\right\}\mathrm{e}^{-\zeta^2} + \frac{4m}{3}\sqrt{\frac{2}{\pi}}\,\mathrm{erf}\big(\sqrt{2}\zeta\big) - \frac{m}{\sqrt{\pi}}\left(1+\frac{4}{9\pi}\right),\\ G_1(\zeta) &= \frac{m}{6\pi}\left[\sqrt{\mathrm{Pr}}(5+3\mathrm{Pr}) - 3(1+\mathrm{Pr})^2\tan^{-1}\left(\frac{1}{\sqrt{\mathrm{Pr}}}\right)\right]\left[\big(1+2\mathrm{Pr}\zeta^2\big)\mathrm{erf}\big(\sqrt{\mathrm{Pr}}\,\zeta\big) + 2\sqrt{\frac{\mathrm{Pr}}{\pi}}\zeta\,\mathrm{e}^{-\mathrm{Pr}\zeta^2}\right]\\ &\quad - \frac{m}{2}\sqrt{\frac{\mathrm{Pr}}{\pi}}\Big[\big(1-2\mathrm{Pr}-\mathrm{Pr}^2\big)\zeta\,\mathrm{e}^{-\mathrm{Pr}\zeta^2}\,\mathrm{erf}\,\zeta - (1+\mathrm{Pr})^2\big(1+2\mathrm{Pr}\zeta^2\big)\int_0^{\zeta}\mathrm{e}^{-\mathrm{Pr}\bar{\zeta}^2}\,\mathrm{erf}\,\bar{\zeta}\;\mathrm{d}\bar{\zeta}\Big]\\ &\quad + \frac{m}{\pi}\sqrt{\mathrm{Pr}}\left[\left(\frac{4}{3}-\frac{1}{2}(1-\mathrm{Pr})\mathrm{e}^{-\zeta^2}\right)\mathrm{e}^{-\mathrm{Pr}\zeta^2} - \frac{1}{6}(5+3\mathrm{Pr})\big(1+2\mathrm{Pr}\zeta^2\big)\right], \end{aligned} \tag{19}$$

where $\mathrm{erf}\,\zeta = (2/\sqrt{\pi})\int_0^{\zeta}\mathrm{e}^{-s^2}\,\mathrm{d}s$ is the error function and $\mathrm{erfc}\,\zeta = 1-\mathrm{erf}\,\zeta$ is the complementary error function, whilst the ordinary differential systems for $F_2(\zeta)$ and $G_2(\zeta)$ have been solved numerically for particular values of the Prandtl number Pr. For the case $\mathrm{Pr}=1$, this expression for $G_1(\zeta)$ reduces to the following simpler form:

$$G_1(\zeta) = m\left(-\frac{1}{2}\,\mathrm{erfc}\,\zeta + \frac{4}{3\pi}\right)\left[\big(1+2\zeta^2\big)\mathrm{erf}\,\zeta + \frac{2}{\sqrt{\pi}}\zeta\,\mathrm{e}^{-\zeta^2}\right] + \frac{4m}{3\pi}\left[-\big(1+2\zeta^2\big)+\mathrm{e}^{-\zeta^2}\right], \tag{20}$$

since this choice for Pr enables the integral in the formula for $G_1(\zeta)$ to be evaluated explicitly.

The first two terms in the solutions for the non-dimensional fluid velocity $(\partial F/\partial\zeta)(\zeta,\tau)$ and temperature $G(\zeta,\tau)$ functions at times $\tau \ll 1$ then follow from Eq. (16) together with

$$\begin{aligned}
F_0'(\zeta) &= \operatorname{erf}\zeta,\\
F_1'(\zeta) &= m\left(\frac{1}{2}-\zeta^2\right)\operatorname{erf}\zeta\operatorname{erfc}\zeta - 2m\left[\frac{1}{3\pi}+\left(1+\frac{2}{3\pi}\right)\zeta^2\right]\operatorname{erfc}\zeta + \frac{m}{\sqrt{\pi}}\left(1+\frac{4}{3\pi}+3\operatorname{erf}\zeta\right)\zeta\,\mathrm{e}^{-\zeta^2}\\
&\quad + \frac{2m}{\pi}\left(-\frac{2}{3}+\mathrm{e}^{-\zeta^2}\right)\mathrm{e}^{-\zeta^2}.
\end{aligned} \tag{21}$$

Hence, the small τ solutions for the non-dimensional fluid velocity $(\partial f/\partial\eta)(\eta,\tau)$ and temperature $g(\eta,\tau)$ functions can be written as follows:

$$\begin{aligned}
\frac{\partial f}{\partial\eta}(\eta,\tau) &= \operatorname{erf}\Big(\frac{\eta}{2\tau^{1/2}}\Big) + m\left\{\left(\frac{1}{2}\tau-\frac{\eta^2}{4}\right)\operatorname{erf}\Big(\frac{\eta}{2\tau^{1/2}}\Big)\operatorname{erfc}\Big(\frac{\eta}{2\tau^{1/2}}\Big) - \left[\frac{2\tau}{3\pi}+\left(1+\frac{2}{3\pi}\right)\frac{\eta^2}{2}\right]\operatorname{erfc}\Big(\frac{\eta}{2\tau^{1/2}}\Big)\right.\\
&\qquad \left. + \frac{1}{2\sqrt{\pi}}\left[1+\frac{4}{3\pi}+3\operatorname{erf}\Big(\frac{\eta}{2\tau^{1/2}}\Big)\right]\eta\tau^{\frac{1}{2}}\,\mathrm{e}^{-\frac{\eta^2}{4\tau}} + \frac{2\tau}{\pi}\left(-\frac{2}{3}+\mathrm{e}^{-\frac{\eta^2}{4\tau}}\right)\mathrm{e}^{-\frac{\eta^2}{4\tau}}\right\}\\
&\quad + F_2\Big(\frac{\eta}{2\tau^{1/2}}\Big)\tau^2+\cdots,\\
g(\eta,\tau) &= \operatorname{erfc}\Big(\frac{\eta}{2\tau^{1/2}}\sqrt{\mathrm{Pr}}\Big) + m\left\{\frac{1}{6\pi}\left[\sqrt{\mathrm{Pr}}(5+3\mathrm{Pr}) - 3(1+\mathrm{Pr})^2\tan^{-1}\Big(\frac{1}{\sqrt{\mathrm{Pr}}}\Big)\right]\right.\\
&\qquad \times\left[\left(\tau+\frac{1}{2}\mathrm{Pr}\eta^2\right)\operatorname{erf}\Big(\frac{\eta}{2\tau^{1/2}}\sqrt{\mathrm{Pr}}\Big) + \sqrt{\frac{\mathrm{Pr}}{\pi}}\eta\tau^{\frac{1}{2}}\,\mathrm{e}^{-\frac{\mathrm{Pr}\eta^2}{4\tau}}\right]\\
&\qquad -\frac{1}{2}\sqrt{\frac{\mathrm{Pr}}{\pi}}\left[\frac{1}{2}(1-2\mathrm{Pr}-\mathrm{Pr}^2)\eta\tau^{\frac{1}{2}}\,\mathrm{e}^{-\frac{\mathrm{Pr}\eta^2}{4\tau}}\operatorname{erf}\Big(\frac{\eta}{2\tau^{1/2}}\Big) - (1+\mathrm{Pr})^2\left(\tau+\frac{1}{2}\mathrm{Pr}\eta^2\right)\right.\\
&\qquad \left.\times\int_0^{\eta/2\tau^{1/2}}\mathrm{e}^{-\mathrm{Pr}\bar{\zeta}^2}\operatorname{erf}\bar{\zeta}\,\partial\bar{\zeta}\right]\\
&\qquad \left.+\frac{1}{\pi}\sqrt{\mathrm{Pr}}\left[\tau\left(\frac{4}{3}-\frac{1}{2}(1-\mathrm{Pr})\mathrm{e}^{-\frac{\eta^2}{4\tau}}\right)\mathrm{e}^{-\frac{\mathrm{Pr}\eta^2}{4\tau}} - \frac{1}{6}(5+3\mathrm{Pr})\left(\tau+\frac{1}{2}\mathrm{Pr}\eta^2\right)\right]\right\}\\
&\quad + G_2\Big(\frac{\eta}{2\tau^{1/2}}\Big)\tau^2+\cdots,
\end{aligned} \tag{22}$$

where the solution for $g(\eta,\tau)$ in the case of $\mathrm{Pr}=1$ reduces to

$$\begin{aligned}
g(\eta,\tau) &= \operatorname{erfc}\Big(\frac{\eta}{2\tau^{1/2}}\Big) + m\left\{\left(\frac{4}{3\pi}-\frac{1}{2}\operatorname{erfc}\Big(\frac{\eta}{2\tau^{1/2}}\Big)\right)\left[\left(\tau+\frac{1}{2}\eta^2\right)\operatorname{erf}\Big(\frac{\eta}{2\tau^{1/2}}\Big) + \frac{1}{\sqrt{\pi}}\eta\tau^{\frac{1}{2}}\,\mathrm{e}^{-\frac{\eta^2}{4\tau}}\right]\right.\\
&\qquad \left. + \frac{4}{3\pi}\left[-\left(\tau+\frac{1}{2}\eta^2\right)+\tau\,\mathrm{e}^{-\frac{\eta^2}{4\tau}}\right]\right\} + G_2\Big(\frac{\eta}{2\tau^{1/2}}\Big)\tau^2+\cdots.
\end{aligned} \tag{23}$$

The solutions of the ordinary differential systems for the functions $F_2(\zeta)$ and $G_2(\zeta)$, arising in the small time series expansions (16), can be achieved using the NAG routine D02HAF. This algorithm solves two-point, boundary-value problems for systems of first-order, ordinary differential equations using a Runge–Kutta–Merson method and a Newton iteration in a shooting and matching technique. In this numerical procedure, the upper range of integration must be specified at some finite value instead of infinity, and we will denote the values of ζ and η corresponding to $\zeta=\infty$ and $\eta=\infty$ by ζ_∞ and η_∞, respectively.

Two quantities of physical interest in this problem are the skin friction coefficient $C_f = \tau_w(\bar{x})/\rho(\bar{u}_e(\bar{x}))^2$ and the local Nusselt number $\mathrm{Nu} = q_w(\bar{x})\bar{x}/k_f(T_w-T_\infty)$, where $\tau_w(\bar{x}) = \mu(\partial\bar{u}/\partial\bar{y})_{\bar{y}=0}$ is the skin friction along the surface, $q_w(\bar{x}) = -k_f(\partial\overline{T}/\partial\bar{y})_{\bar{y}=0}$ is the surface heat flux, ρ is the fluid density, k_f is the thermal conductivity of the fluid, and μ is the coefficient of viscosity. By introducing the non-dimensional variables (2) and the transformation (8), the skin friction coefficient $C_f\mathrm{Re}_x^{1/2}$ and the local Nusselt number $\mathrm{Nu}/\mathrm{Re}_x^{1/2}$ can now be expressed as

$$C_f\mathrm{Re}_x^{1/2} = \frac{\partial^2 f}{\partial\eta^2}(0,\tau) = \frac{1}{2\tau^{1/2}}\frac{\partial^2 F}{\partial\zeta^2}(0,\tau) = \frac{1}{\sqrt{\pi}}\tau^{-\frac{1}{2}} + \frac{m}{\sqrt{\pi}}\left(1+\frac{4}{3\pi}\right)\tau^{\frac{1}{2}} + \frac{1}{2}F_2''(0)\tau^{\frac{3}{2}}+\cdots,$$

Table 1
The variation of (a) $F_2''(0)$ with the parameter m, and (b) $G_2'(0)$ with the parameters $m = \beta/(2-\beta)$ and Pr, which occur in the small time solution (24)

(a)			(b)				
			Pr				
β	m		0.72	1	2	5	10
	m^*	−0.0093527	−0.0039771	−0.0051209	−0.0075477	−0.0103737	−0.0120473
	−0.05	−0.0043664	−0.0019832	−0.0025766	−0.0038377	−0.0053081	−0.0061794
0	0	0.0	0.0	0.0	0.0	0.0	0.0
$\frac{1}{6}$	$\frac{1}{11}$	0.0028385	0.0022382	0.0030701	0.0048509	0.0069402	0.0081815
$\frac{1}{3}$	$\frac{1}{5}$	−0.0024428	0.0025945	0.0040042	0.0070499	0.0106513	0.0127983
$\frac{1}{2}$	$\frac{1}{3}$	−0.0217678	−0.0004211	0.0010715	0.0043712	0.0083468	0.0107356
1	1	−0.3307504	−0.0724423	−0.0808175	−0.0975653	−0.1160398	−0.1267155
$\frac{4}{3}$	2	−1.4578424	−0.3584214	−0.4137308	−0.5271670	−0.6553197	−0.7301979

$$\frac{\mathrm{Nu}}{\mathrm{Re}_x^{1/2}} = -\frac{\partial g}{\partial \eta}(0,\tau) = -\frac{1}{2\tau^{1/2}}\frac{\partial G}{\partial \zeta}(0,\tau)$$
$$= \sqrt{\frac{\mathrm{Pr}}{\pi}}\tau^{-\frac{1}{2}} + \frac{m}{\pi}\sqrt{\frac{\mathrm{Pr}}{\pi}}\left[(1+\mathrm{Pr})^2\tan^{-1}\left(\frac{1}{\sqrt{\mathrm{Pr}}}\right) - \frac{1}{3}\sqrt{\mathrm{Pr}}(5+3\mathrm{Pr})\right]\tau^{\frac{1}{2}} - \frac{1}{2}G_2'(0)\tau^{\frac{3}{2}} + \cdots, \tag{24}$$

for $\tau \ll 1$, where $\mathrm{Re}_x = \bar{u}_e(\bar{x})\frac{\bar{x}}{\bar{\nu}}$ is the local Reynolds number.

In Table 1 we present the variation of $F_2''(0)$ and $G_2'(0)$, which occur in the small time solution (24) for the non-dimensional skin friction coefficient and the local Nusselt number, with the parameters m and Pr. The small time solution (24) is presented in Section 6 for different numbers of terms and its ranges of validity will be determined as a function of m and Pr. The case of $m = m^*$ represents the value of m at which the laminar boundary-layer breaks away from the surface and this limiting value is discussed in depth in Section 4. Also included in this table are the values of $F_2''(0)$ and $G_2'(0)$ for the case of $\beta = 4/3$, $m = 2$ obtained from the steady-state Falkner–Skan solution.

4. Large time solution, $\tau \to \infty$

The transport of energy becomes steady as $\tau \to \infty$ and, hence, $f(\eta,\tau) = f_\infty(\eta)$ and $g(\eta,\tau) = g_\infty(\eta)$, say, so that the Eqs. (9) and (10) reduce to the following ordinary differential equations:

$$f_\infty''' + \frac{1}{2}(m+1)f_\infty f_\infty'' + m\left(1 - f_\infty'^2\right) = 0, \tag{25}$$

$$\frac{1}{\mathrm{Pr}}g_\infty'' + \frac{1}{2}(m+1)f_\infty g_\infty' = 0, \tag{26}$$

which must be solved subject to the boundary conditions

$$f_\infty(0) = 0, \qquad f_\infty'(0) = 0, \qquad g_\infty(0) = 1, \qquad f_\infty'(\eta) \to 1, \quad g_\infty(\eta) \to 0 \quad \text{as } \eta \to \infty, \tag{27}$$

where primes now denote differentiation with respect to η.

The stream function $f_\infty(\eta)$ is the well-known Falkner–Skan solution and the properties of this solution, as a function of the parameter m, have been discussed in numerous papers, see Lin and Lin [25]. In this paper, we are mainly interested in the standard, Blasius-like solutions to the Falkner–Skan equation (25), although other solutions, mostly exhibiting regions of reversed flow near to the surface, have been obtained for most values of m, see, for example, Heeg et al. [26] and the references therein.

The Blasius-like solutions exist for each value of m in the range $m^* \leqslant m < \infty$, where m^* determines the point at which the laminar boundary-layer breaks away from the surface, and satisfy both $0 < f_\infty'(\eta) < 1$ and $f_\infty''(\eta) > 0$ for $0 < \eta < \infty$. Thus, $f_\infty''(0) = 0$ at $m = m^*$ and, in this case, $f_\infty''(0)$ increases monotonically with m for $m > m^*$, see Stewartson [27] and Section 4.1. Here, it is to be understood that the boundary condition (27) on $f_\infty'(\eta)$ as $\eta \to \infty$ requires that $1 - f_\infty'(\eta) \to 0$ exponentially.

Hartree [28] investigated the behaviour of the non-dimensional skin friction coefficient $f''_\infty(0)$ around $m = m^*$ and showed that this limiting value marks a definite discontinuity in the relation between m and $f''_\infty(0)$. As $m \to (m^*)^+$, the non-dimensional skin friction coefficient was shown numerically to approach zero as $O(m - m^*)^{1/2}$. This singularity was also demonstrated mathematically to exist by Banks and Drazin [29], see Section 4.2. Furthermore, for $m^* < m < 0$, the Falkner–Skan equation (25) has precisely two solutions, where the second solution exhibits reversed flow near to the surface, see Section 4.5.

In the following sections, we briefly describe the variations in the solutions for the non-dimensional skin friction coefficient $f''_\infty(0)$ and the surface heat flux $g'_\infty(0)$ in the cases of $m \gg 1$, $m \to (m^*)^+$, and $|m| \ll 1$, together with the influence of the parameter m on the fluid velocity $f'_\infty(\eta)$ and the fluid temperature $g_\infty(\eta)$ for this large time, steady-state solution at different values of the Prandtl number Pr. The solutions to all of the ordinary differential systems derived have been achieved using the NAG routines D02HAF and D02HBF, the latter routine providing a generalisation of D02HAF in which parameters other than the boundary values are to be determined.

4.1. Steady solution for $m \gg 1$

For large values of m, the solutions of the differential systems (25)–(27) have the following form:

$$f_\infty(\eta) = m^{-\frac{1}{2}} \sum_{i=0}^{\infty} \bar{f}_{\infty,i}(\bar{\eta}) m^{-i}, \qquad g_\infty(\eta) = \sum_{i=0}^{\infty} \bar{g}_{\infty,i}(\bar{\eta}) m^{-i}, \qquad \bar{\eta} = m^{\frac{1}{2}}\eta. \tag{28}$$

By substituting these expressions into the systems (25)–(27) and equating coefficients of powers of m, we obtain ordinary differential systems governing the solutions for the coefficient functions $\bar{f}_{\infty,i}(\bar{\eta})$ and $\bar{g}_{\infty,i}(\bar{\eta})$. The first two pairs of coupled, ordinary differential equations

$$\bar{f}'''_{\infty,0} + \frac{1}{2}\bar{f}_{\infty,0}\bar{f}''_{\infty,0} + 1 - \bar{f}'^2_{\infty,0} = 0, \qquad \frac{1}{\mathrm{Pr}}\bar{g}''_{\infty,0} + \frac{1}{2}\bar{f}_{\infty,0}\bar{g}'_{\infty,0} = 0, \tag{29}$$

$$\begin{aligned} &\bar{f}'''_{\infty,1} + \frac{1}{2}\big(\bar{f}_{\infty,0}\bar{f}''_{\infty,0} + \bar{f}_{\infty,0}\bar{f}''_{\infty,1} + \bar{f}''_{\infty,0}\bar{f}_{\infty,1}\big) - 2\bar{f}'_{\infty,0}\bar{f}'_{\infty,1} = 0, \\ &\qquad \frac{1}{\mathrm{Pr}}\bar{g}''_{\infty,1} + \frac{1}{2}\big(\bar{f}_{\infty,0}\bar{g}'_{\infty,0} + \bar{f}_{\infty,0}\bar{g}'_{\infty,1} + \bar{f}_{\infty,1}\bar{g}'_{\infty,0}\big) = 0, \end{aligned} \tag{30}$$

where primes denote differentiation with respect to $\bar{\eta}$, together with the boundary conditions

$$\begin{aligned} &\bar{f}_{\infty,0}(0) = 0, \quad \bar{f}'_{\infty,0}(0) = 0, \quad \bar{f}_{\infty,1}(0) = 0, \quad \bar{f}'_{\infty,1}(0) = 0, \quad \bar{g}_{\infty,0}(0) = 1, \quad \bar{g}_{\infty,1}(0) = 0, \\ &\bar{f}'_{\infty,0}(\bar{\eta}) \to 1, \quad \bar{f}'_{\infty,1}(\bar{\eta}) \to 0, \quad \bar{g}_{\infty,0}(\bar{\eta}) \to 0, \quad \bar{g}_{\infty,1}(\bar{\eta}) \to 0 \quad \text{as } \bar{\eta} \to \infty, \end{aligned} \tag{31}$$

can then be solved to determine the solutions for $\bar{f}_{\infty,0}(\bar{\eta})$, $\bar{g}_{\infty,0}(\bar{\eta})$, $\bar{f}_{\infty,1}(\bar{\eta})$, and $\bar{g}_{\infty,1}(\bar{\eta})$.

The steady-state non-dimensional skin friction coefficient and local Nusselt number are given by

$$C_f \mathrm{Re}_x^{1/2} = \left.\frac{\partial^2 f_\infty(\eta)}{\partial\eta^2}\right|_{\eta=0} = m^{\frac{1}{2}}\bar{f}''_{\infty,0}(0) + m^{-\frac{1}{2}}\bar{f}''_{\infty,1}(0) + O\big(m^{-3/2}\big), \tag{32}$$

$$\frac{\mathrm{Nu}}{\mathrm{Re}_x^{1/2}} = -\left.\frac{\partial g_\infty(\eta)}{\partial\eta}\right|_{\eta=0} = -m^{\frac{1}{2}}\bar{g}'_{\infty,0}(0) - m^{-\frac{1}{2}}\bar{g}'_{\infty,1}(0) + O\big(m^{-3/2}\big), \tag{33}$$

for $m \gg 1$, where

$$\bar{f}''_{\infty,0}(0) = 1.1930434, \qquad \bar{f}''_{\infty,1}(0) = 0.0391436, \tag{34}$$

and the values of $\bar{g}'_{\infty,0}(0)$ and $\bar{g}'_{\infty,1}(0)$ have been calculated using the NAG routine D02HAF for different values of Pr.

4.2. Steady solution as $m \to (m^*)^+$

The behaviour of the non-dimensional skin friction coefficient $f''_\infty(0)$ in the vicinity of $m = m^*$, with $m > m^*$, was investigated by Hartree [28]. The discontinuity $m = m^*$, at which $f''_\infty(0) = 0$, was shown to be approached as $O(m - m^*)^{1/2}$, which suggests that the solutions of the ordinary differential systems (25)–(27), as $m \to (m^*)^+$, should be sought in the following form:

$$f_\infty(\eta) = \sum_{i=0}^{\infty} f^*_{\infty,i}(\eta)(m - m^*)^{\frac{i}{2}}, \qquad g_\infty(\eta) = \sum_{i=0}^{\infty} g^*_{\infty,i}(\eta)(m - m^*)^{\frac{i}{2}}. \tag{35}$$

By substituting these expressions for $f_\infty(\eta)$ and $g_\infty(\eta)$ into the systems (25)–(27), and equating coefficients of powers of $(m-m^*)^{1/2}$, we obtain ordinary differential systems governing the solutions for the coefficient functions $f^*_{\infty,i}(\eta)$ and $g^*_{\infty,i}(\eta)$. The first two pairs of the resulting coupled, ordinary differential systems are as follows:

$$f^{*\prime\prime\prime}_{\infty,0} + \frac{1}{2}(m^*+1)f^*_{\infty,0}f^{*\prime\prime}_{\infty,0} + m^*\bigl(1 - f^{*\prime 2}_{\infty,0}\bigr) = 0, \qquad \frac{1}{\mathrm{Pr}}g^{*\prime\prime}_{\infty,0} + \frac{1}{2}(m^*+1)f^*_{\infty,0}g^{*\prime}_{\infty,0} = 0, \tag{36}$$

$$\begin{aligned} &f^{*\prime\prime\prime}_{\infty,1} + \frac{1}{2}(m^*+1)\bigl(f^*_{\infty,0}f^{*\prime\prime}_{\infty,1} + f^{*\prime\prime}_{\infty,0}f^*_{\infty,1}\bigr) - 2m^*f^{*\prime}_{\infty,0}f^{*\prime}_{\infty,1} = 0,\\ &\frac{1}{\mathrm{Pr}}g^{*\prime\prime}_{\infty,1} + \frac{1}{2}(m^*+1)\bigl(f^*_{\infty,0}g^{*\prime}_{\infty,1} + f^*_{\infty,1}g^{*\prime}_{\infty,0}\bigr) = 0, \end{aligned} \tag{37}$$

where primes denote differentiation with respect to η, which must be solved subject to the boundary conditions

$$\begin{aligned} &f^*_{\infty,0}(0) = 0, \quad f^{*\prime}_{\infty,0}(0) = 0, \quad f^*_{\infty,1}(0) = 0, \quad f^{*\prime}_{\infty,1}(0) = 0, \quad g^*_{\infty,0}(0) = 1, \quad g^*_{\infty,1}(0) = 0,\\ &f^{*\prime}_{\infty,0}(\eta) \to 1, \quad f^{*\prime}_{\infty,1}(\eta) \to 0, \quad g^*_{\infty,0}(\eta) \to 0, \quad g^*_{\infty,1}(\eta) \to 0 \quad \text{as } \eta \to \infty. \end{aligned} \tag{38}$$

The ordinary differential equation (36) for $f^*_{\infty,0}(\eta)$, subject to the appropriate boundary conditions (38), can be solved using the NAG routine D02HBF. The parameter $m^* = -0.0904285623$ can then be determined by imposing the additional constraint that $f''_\infty(0) = 0$ at this discontinuity.

The fact that $f''_\infty(0) = f^{*\prime\prime}_{\infty,0}(0) = 0$ at $m = m^*$ allows us to recognise the solution of the ordinary differential equation (37) for $f^*_{\infty,1}(\eta)$, subject to the associated boundary conditions (38), to have the form

$$f^*_{\infty,1}(\eta) = af^{*\prime}_{\infty,0}(\eta), \tag{39}$$

where a is an arbitrary constant. Banks and Drazin [29] showed that the value of a can be determined by requiring that the problem for $f^*_{\infty,2}(\eta)$ is soluble. Subsequently, we obtain that $a = f^*_{\infty,1}(\infty) = 9.7928138$ by solving the first three ordinary differential systems for $f^*_{\infty,0}(\eta)$, $f^*_{\infty,1}(\eta)$, and $f^*_{\infty,2}(\eta)$ using the NAG routine D02HBF. It is also evident that the further solutions for $f^*_{\infty,2}(\eta)$ and $f^*_{\infty,3}(\eta)$ can be achieved by requiring that the first five ordinary differential systems are soluble.

The steady-state non-dimensional skin friction coefficient and local Nusselt number are given by

$$C_f\mathrm{Re}_x^{1/2} = f''_\infty(0) = f^{*\prime\prime}_{\infty,1}(0)(m-m^*)^{\frac{1}{2}} + f^{*\prime\prime}_{\infty,2}(0)(m-m^*) + f^{*\prime\prime}_{\infty,3}(0)(m-m^*)^{\frac{3}{2}} + O(m-m^*)^2, \tag{40}$$

$$\frac{\mathrm{Nu}}{\mathrm{Re}_x^{1/2}} = -g'_\infty(0) = -g^{*\prime}_{\infty,0}(0) - g^{*\prime}_{\infty,1}(0)(m-m^*)^{\frac{1}{2}} - g^{*\prime}_{\infty,2}(0)(m-m^*) - g^{*\prime}_{\infty,3}(0)(m-m^*)^{\frac{3}{2}} + O(m-m^*)^2, \tag{41}$$

as $m \to (m^*)^+$. As presented by Hartree [28], the graphs of the non-dimensional skin friction coefficient and the local Nusselt number, as functions of m, for values of m close to m^* have two branches, reversed flow corresponding to points on the lower branch and arising from the negative square root in Eqs. (40) and (41). Here

$$f^{*\prime\prime}_{\infty,1}(0) = -am^* = 0.8855501, \qquad f^{*\prime\prime}_{\infty,2}(0) = 1.3126251, \qquad f^{*\prime\prime}_{\infty,3}(0) = -2.6667748, \tag{42}$$

and the values of $g^{*\prime}_{\infty,0}(0)$, $g^{*\prime}_{\infty,1}(0)$, $g^{*\prime}_{\infty,2}(0)$, and $g^{*\prime}_{\infty,3}(0)$ have been calculated using the NAG routine D02HBF for different values of Pr.

4.3. Steady solution in the vicinity of $m = 0$

The solutions of the ordinary differential systems (25)–(27) in the vicinity of $m = 0$ (Blasius problem) have the following form:

$$f_\infty(\eta) = \sum_{i=0}^{\infty} f^0_{\infty,i}(\eta)m^i, \qquad g_\infty(\eta) = \sum_{i=0}^{\infty} g^0_{\infty,i}(\eta)m^i. \tag{43}$$

By substituting these expressions into the systems (25)–(27) and equating coefficients of powers of m, we obtain ordinary differential systems governing the solutions for the coefficient functions $f^0_{\infty,i}(\eta)$ and $g^0_{\infty,i}(\eta)$. The first two pairs of the resulting coupled, ordinary differential systems are as follows:

$$f^{0'''}_{\infty,0} + \frac{1}{2} f^{0}_{\infty,0} f^{0''}_{\infty,0} = 0, \qquad \frac{1}{\mathrm{Pr}} g^{0''}_{\infty,0} + \frac{1}{2} f^{0}_{\infty,0} g^{0'}_{\infty,0} = 0, \tag{44}$$

$$f^{0'''}_{\infty,1} + \frac{1}{2}\left(f^{0}_{\infty,0} f^{0''}_{\infty,1} + f^{0''}_{\infty,0} f^{0}_{\infty,1}\right) + \frac{1}{2} f^{0}_{\infty,0} f^{0''}_{\infty,0} + 1 - f^{0'2}_{\infty,0} = 0,$$

$$\frac{1}{\mathrm{Pr}} g^{0''}_{\infty,1} + \frac{1}{2}\left(f^{0}_{\infty,0} g^{0'}_{\infty,1} + f^{0}_{\infty,1} g^{0'}_{\infty,0}\right) + \frac{1}{2} f^{0}_{\infty,0} g^{0'}_{\infty,0} = 0, \tag{45}$$

where primes denote differentiation with respect to η, which must be solved subject to the boundary conditions

$$f^{0}_{\infty,0}(0) = 0, \qquad f^{0'}_{\infty,0}(0) = 0, \qquad f^{0}_{\infty,1}(0) = 0, \qquad f^{0'}_{\infty,1}(0) = 0, \qquad g^{0}_{\infty,0}(0) = 1, \qquad g^{0}_{\infty,1}(0) = 0,$$

$$f^{0'}_{\infty,0}(\eta) \to 1, \qquad f^{0'}_{\infty,1}(\eta) \to 0, \qquad g^{0}_{\infty,0}(\eta) \to 0, \qquad g^{0}_{\infty,1}(\eta) \to 0 \qquad \text{as } \eta \to \infty. \tag{46}$$

It should be noted that the above equation satisfied by $f^{0}_{\infty,0}(\eta)$ is the well-known Blasius equation.

The steady-state non-dimensional skin friction coefficient and local Nusselt number are given by

$$C_f \mathrm{Re}_x^{1/2} = f''_{\infty}(0) = f^{0''}_{\infty,0}(0) + m f^{0''}_{\infty,1}(0) + m^2 f^{0''}_{\infty,2}(0) + O\left(m^3\right), \tag{47}$$

$$\frac{\mathrm{Nu}}{\mathrm{Re}_x^{1/2}} = -g'_{\infty}(0) = -g^{0'}_{\infty,0}(0) - m g^{0'}_{\infty,1}(0) - m^2 g^{0'}_{\infty,2}(0) + O\left(m^3\right), \tag{48}$$

in the vicinity of $m = 0$, where

$$f^{0''}_{\infty,0}(0) = f''_{\infty}(0) = 0.3320573, \qquad f^{0''}_{\infty,1}(0) = 2.0029918, \qquad f^{0''}_{\infty,2}(0) = -5.2648717, \tag{49}$$

and the values of $g^{0'}_{\infty,0}(0)$, $g^{0'}_{\infty,1}(0)$, and $g^{0'}_{\infty,2}(0)$ have been calculated using the NAG routine D02HAF for different values of Pr. We notice that the value of $f''_{\infty}(0)$ coincides with that obtained by Blasius, see Lin and Lin [25].

4.4. Steady solution for $m^* \leqslant m < \infty$

To describe the large time, steady-state solution to the transient heat transfer problem described in this paper, we are mainly concerned with the Blasius-like solutions to the system (25)–(27). As explained in this section, such solutions exist for $m^* \leqslant m < \infty$ and the NAG routine D02HAF can be employed to numerically determine the complete behaviour of the non-dimensional skin friction coefficient and the local Nusselt number over this range. These Blasius-like numerical solutions, together with the solutions exhibiting regions of reversed flow near to the surface, are compared to the various asymptotic behaviours derived in Sections 4.1 to 4.3 in Fig. 2, for different values of the Prandtl number Pr. It will become evident from Fig. 3, see Section 4.5, that the value of η_∞ at which those boundary conditions (27) which are valid as $\eta \to \infty$ are to be applied depends crucially upon the chosen value of m, particularly near to m^* and for the reversed flow cases.

Fig. 2(a) shows the variation of $f''_{\infty}(0)$ and $g'_{\infty}(0)$ at large values of m in comparison to the 1- and 2-term large m expansions presented in Eqs. (32) and (33) for the non-dimensional skin friction coefficient and the local Nusselt number, respectively. These 1-term solutions provide a reasonable approximation to $f''_{\infty}(0)$ for $m \geqslant 5$, but are relatively poor for the displayed interval of m values when the $g'_{\infty}(0)$ solution is considered. A significant improvement in the validity of the large m approximation is observed when the second term in each expansion is included. In the approximation for $f''_{\infty}(0)$, the 2-term expansion (32) is graphically indistinguishable from the corresponding numerical solution for $m \gtrsim 0.13$, and this fact is emphasized in Fig. 2(b), where the same asymptotic behaviour has been included within an enhanced view of the solutions in the vicinity of $m = 0$. In the approximation for $g'_{\infty}(0)$, the 2-term expansion (33) provides a graphically accurate representation for $m \gtrsim 4$.

Fig. 2(b) shows the variation of $f''_{\infty}(0)$ and $g'_{\infty}(0)$ in the vicinity of $m = 0$ in comparison to the 3-term expansions (47) and (48) for the non-dimensional skin friction coefficient and the local Nusselt number, respectively. These quadratic approximations to the behaviour of $f''_{\infty}(0)$ and $g'_{\infty}(0)$ are only graphically indistinguishable from the corresponding numerical solutions over the interval $-0.03 \lesssim m \lesssim 0.05$.

Fig. 2(c) shows the behaviour of $f''_{\infty}(0)$ and $g'_{\infty}(0)$ as $m \to (m^*)^+$, where m^* defines the point at which the boundary-layer breaks away from the surface. As discussed in Section 4.2, the numerical solutions for $m^* < m < 0$ have two branches, the reversed flow solutions corresponding to those branches existing over the range $m^* < m < 0$ only. The expansions (40) and (41) are valid as $m \to (m^*)^+$ and have been presented in Fig. 2(c) using the first two and four terms, namely the terms up to $O(m - m^*)^{1/2}$ and $O(m - m^*)^{3/2}$, respectively, with the term of $O(m - m^*)^0$ in Eq. (40) being identically zero. The 2-term approximations are only valid over a very small interval beyond $m = m^*$, whilst the inclusion of the third and then the fourth terms are each successful in significantly improving the upper range of validity of the expansions. The 4-term approximations are valid up to $m \approx -0.065$ for the $f''_{\infty}(0)$ solution and up to between $m \approx -0.08$ and $m \approx -0.03$ for the $g'_{\infty}(0)$ solution, the precise value depending on which branch is being considered and the value of Pr, there being a general decrease in this upper range with increasing values of Pr.

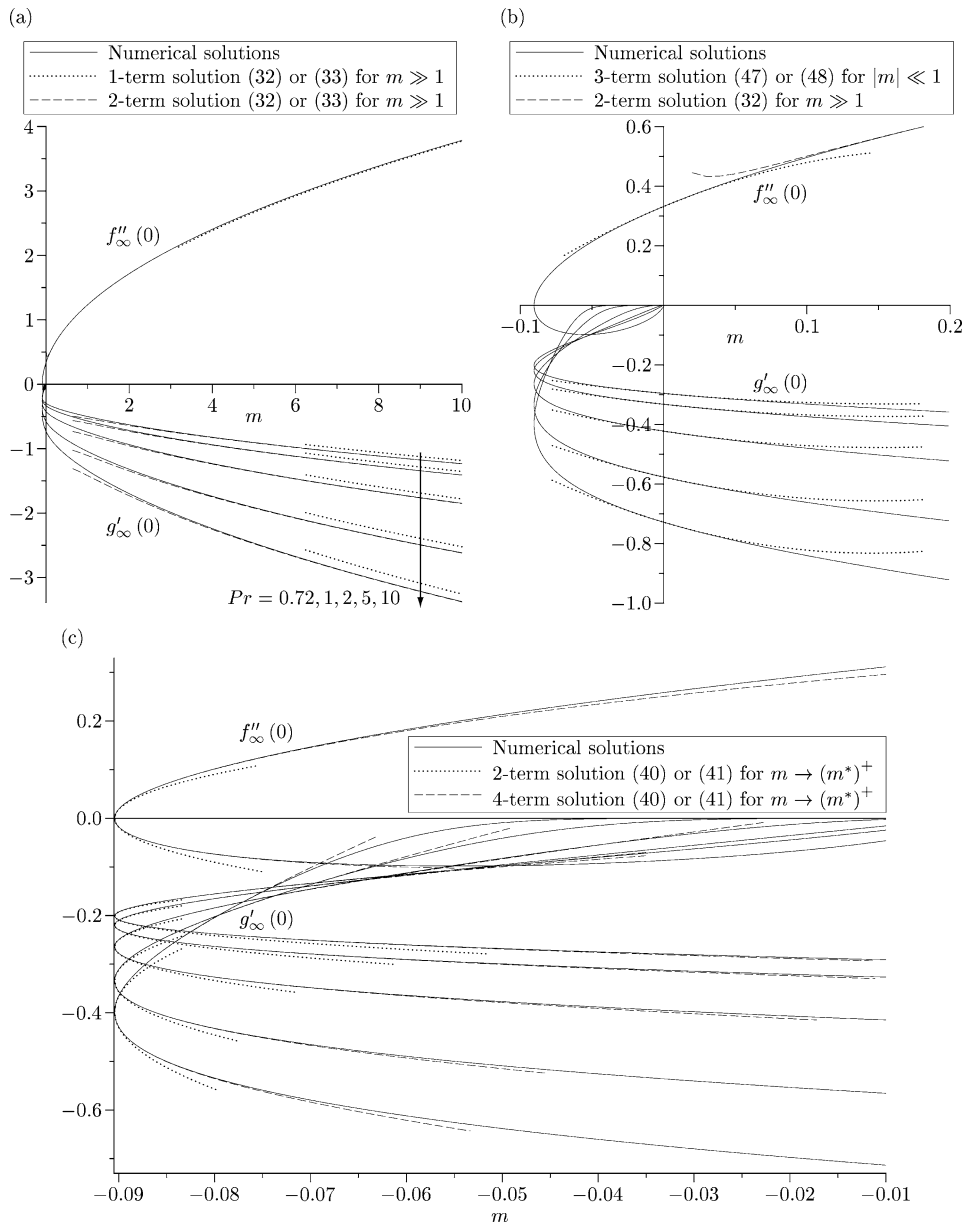

Fig. 2. The variation of $f''_\infty(0)$ with m, and $g'_\infty(0)$ with m at different values of Pr, (a) for large values of m, (b) in the vicinity of $m = 0$, and (c) close to the value $m = m^*$.

4.5. *Large time fluid velocity and temperature profiles*

The large time, steady-state profiles of the non-dimensional fluid velocity function $f'_\infty(\eta)$ and the fluid temperature function $g_\infty(\eta)$ are presented in Fig. 3 at different values of m for the case $\mathrm{Pr} = 1$. The Blasius-like numerical solutions to Eqs. (25)–(27) are illustrated for a variety of values of m over the range $m^* \leqslant m \leqslant 2$, whilst the reversed flow cases are shown for four values of m within the range $m^* < m < 0$. Both the thermal and the velocity boundary-layer thicknesses for the Blasius-like numerical solutions are observed to reduce as the value of m increases. For the reversed flow cases, there is a significant increase in both the thermal and the velocity boundary-layer thicknesses, confirming the need to accordingly increase the value of η_∞, as discussed in Section 4.4. The corresponding non-dimensional fluid temperature profiles for other values of Pr show the same tendencies and, therefore, have not been presented here. The effect of varying Pr can be seen in Fig. 4.

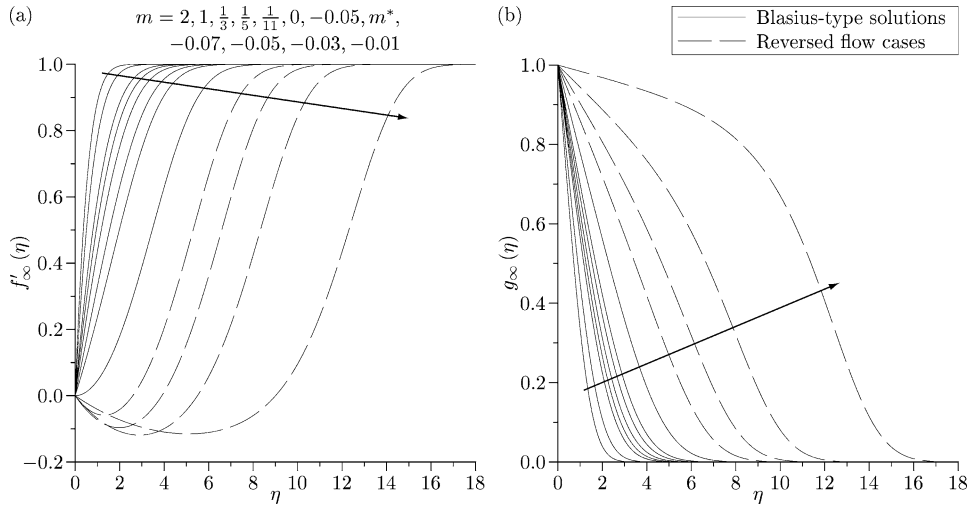

Fig. 3. Large time, steady-state, non-dimensional (a) fluid velocity $f'_\infty(\eta)$ and (b) fluid temperature $g_\infty(\eta)$ profiles at different values of m, including reversed flow cases, for $\mathrm{Pr} = 1$.

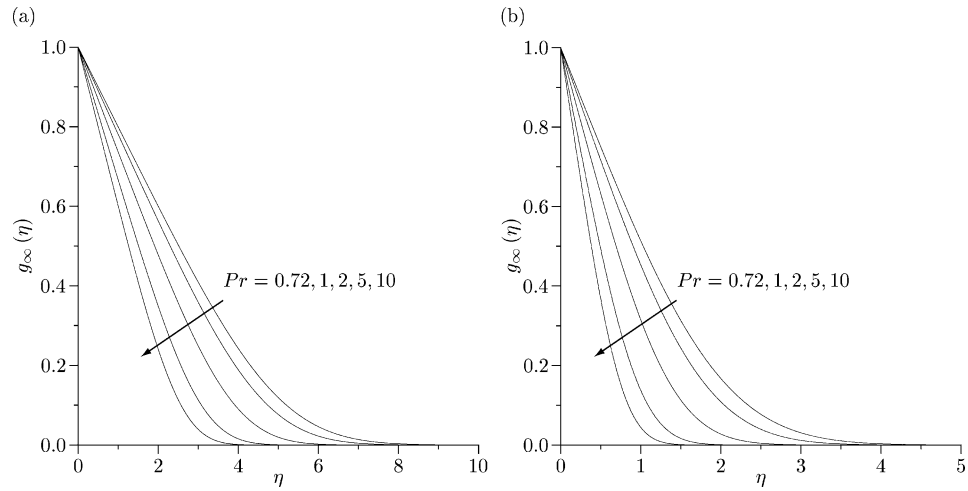

Fig. 4. Large time, steady-state, non-dimensional fluid temperature $g_\infty(\eta)$ profiles at different values of Pr when (a) $m = m^*$ and (b) $m = 1$.

The large time, steady-state profiles of the non-dimensional fluid temperature $g_\infty(\eta)$ are presented in Figs. 4(a) and (b) for $m = m^*$ and $m = 1$, respectively, at the five different values of $\mathrm{Pr} = 0.72$, 1, 2, 5, and 10. As expected, the thermal boundary-layer thickness is observed to decrease as the value of Pr is increased. Again, the corresponding non-dimensional fluid temperature profiles for other values of m show the same tendencies and, therefore, have not been presented here.

5. Numerical solutions

Initially the transient effects due to the imposition of a constant temperature at the surface are confined to a thin fluid region near to this surface and are described by the small time solution developed in Section 3. These effects continue to penetrate outwards through the initial boundary-layer and ultimately evolve into a steady-state flow. In order to match these small and large time solutions, we now develop a numerical solution of the governing boundary-layer equations (4)–(6).

The evolution of the pairs of functions $\partial F/\partial\zeta$, G and $\partial f/\partial\eta$, g are separately governed by the pairs of coupled partial differential equations (13), (14) and (9), (10), respectively, which are each parabolic and thus can be integrated numerically using a step-by-step method similar to that described by Merkin [18], provided that the coefficients of $\partial^2 F/\partial\zeta\partial\tau$, $\partial G/\partial\tau$, $\partial^2 f/\partial\eta\partial\tau$, and $\partial g/\partial\tau$ remain positive throughout the solution domain. This marching method enables the solution at time

$\tau = 0$, described by the functions $F_0(\zeta)$, $G_0(\zeta)$ in Eq. (19), for $\zeta \geqslant 0$, to proceed in time. For $m \geqslant 1$, this forward integration can be continued towards the steady-state solution profiles. However, for $m < 1$, the marching method only provides a numerical solution for $\tau \leqslant \tau_n^*$, where τ_n^* is the time at which the above-mentioned coefficients first become negative in the numerical procedure. The value of τ_n^* will be slightly less than the precise time τ_p^* at which these coefficients first change sign at the outer edge of the boundary-layer, namely

$$\tau_n^* < \tau_p^* = \frac{1}{1-m}, \tag{50}$$

for $m < 1$, to within one time increment of the numerical scheme. Physically (when $m < 1$), as well as mathematically, we would expect that $\tau_n^* = 1/(1-m)$, since for $\tau < 1/(1-m)$ the disturbance from the leading edge has not been felt. The disturbance travels fastest at the outer edge of the boundary-layer and, therefore, it is first encountered at such locations when $\tau = 1/(1-m)$.

The application of the step-by-step scheme to Eqs. (13) and (14) enables the accurate evolution of the temperature profiles to be determined over a developing boundary-layer whose width increases with time. If ζ_∞ and η_∞ are interpreted as being finite values of the spatial variables at which the associated boundary conditions are to be applied, then at the exact time $\tilde{\tau}_p = (\eta_\infty/(2\zeta_\infty))^2$ we must transfer to the step-by-step scheme applied to Eqs. (9) and (10). We again adopt the notation $\tilde{\tau}_n$ to denote the corresponding value of τ which is actually reached in our numerical techniques.

In order to accurately evaluate the initial evolution of the non-dimensional fluid velocity function $\Phi(\zeta,\tau) = (\partial F/\partial\zeta)(\zeta,\tau)$ and the fluid temperature function $G(\zeta,\tau)$ we apply the direct, forward integration scheme to the integro-differential form of Eqs. (13) and (14), following the formulation described in Harris et al. [20,21,23]. The finite spatial domain is divided into N^ζ equal grid spacings of length $h^\zeta = \zeta_\infty/N^\zeta$ and a variable time step is used. To accurately describe the initial evolution, the time increment $\Delta\tau_0$ at time $\tau = 0$ is set to some prescribed small value and subsequently a time step doubling procedure is adopted to reduce the computations at later times. Based upon the fluid velocity and temperature profiles at the final time $\tilde{\tau}_n$ reached in this numerical scheme, we now apply the step-by-step method to Eqs. (9) and (10) and continue towards the steady-state solution or the time $\tau_p^* = 1/(1-m)$, according as to whether $m \geqslant 1$ or $m < 1$, respectively. The numerical formulation used in the paper by Harris et al. [20,21,23] is employed, based upon N^η equal grid spacings for the spatial discretisation.

In the cases for which $m < 1$, at the time $\tau = \tau_n^*$ the forward integration approach breaks down and the coefficients of $\partial^2 f/\partial\eta\partial\tau$ and $\partial g/\partial\tau$ in the governing equations (9) and (10), respectively, are tending towards negative values as $\eta \to \infty$. Based upon the profiles $(\partial f/\partial\eta)(\eta,\tau_n^*)$ and $g(\eta,\tau_n^*)$ at this time and the asymptotic steady-state profiles $f_\infty(\eta)$, $f'_\infty(\eta)$, and $g_\infty(\eta)$, defined as the solution of the system of Eqs. (25)–(27), we complete the numerical integration and derive a solution over $\tau_n^* < \tau < \infty$ by adopting a matching approach. The matching technique originated by Dennis [19] has been successfully applied by the present authors to some related heat transfer problems, see Harris et al. [20–24], wherein comprehensive details of this iterative approach are presented. In the finite-difference approximation to Eqs. (9) and (10), we replace the time derivatives within the terms $\partial^2 f/\partial\eta\partial\tau$ and $\partial g/\partial\tau$ by either a backward or forward difference, depending on whether their coefficient $1+(m-1)\tau\partial f/\partial\eta$ is positive or negative, respectively, to achieve a convergent solution using standard iterative techniques. At some large, but finite, time $\tau = \tau_\infty$ the solution is given by the steady-state analysis. The value of τ_∞ may be varied, but must be taken to be large enough for any further increase to have a negligible effect on the whole solution for $\tau_n^* < \tau < \tau_\infty$.

6. Results and discussion

In the discussion of the parameters within the numerical procedures for determining the transient fluid velocity and temperature fields which follows, we concentrate mainly on the case when the Prandtl number $\mathrm{Pr} = 1$ and $m = 1/5$, namely a wedge angle of 60°. Required alterations to these parameters are then discussed with reference to variations in Pr and m separately.

6.1. *Results for* $\mathrm{Pr} = 1$ *and* $m = 1/5$

The restriction to a finite-dimensional ζ space was achieved by taking $\zeta_\infty = 8$ for $\mathrm{Pr} = 1$ and $m = 1/5$, and thus the precise time at which the transfer to the step-by-step method in η, τ variable takes place is $\tilde{\tau}_p = 0.5625$, taking $\eta_\infty = 12$. The effect on the forward integration numerical schemes of increasing the values of ζ_∞ and η_∞, whilst keeping the corresponding spatial mesh sizes h^ζ and h^η, respectively, constant, was investigated and it was concluded that the results for the non-dimensional fluid velocity and temperature profiles, together with the evolutions of the non-dimensional skin friction coefficient and the local Nusselt number, were graphically indistinguishable from those presented in the figures within this paper. Moreover, it has been observed that the initial evolution of the non-dimensional skin friction coefficient and the local Nusselt number are accurate to eight decimal places with respect to increases in the value of ζ_∞, whilst, in the large time, steady-state solutions for

Table 2
The values of (a) the non-dimensional skin friction coefficient $C_f \mathrm{Re}_x^{1/2} = (\partial^2 f/\partial\eta^2)(0,\tau)$ and (b) the local Nusselt number $\mathrm{Nu}/\mathrm{Re}_x^{1/2} = -(\partial g/\partial\eta)(0,\tau)$ when $\mathrm{Pr} = 1$, for the case $m = 1/5$, obtained using different spatial grid sizes $N = N^{\zeta} = N^{\eta}$, in comparison to the small time solution (24)

(a)

	N						Small τ solution	
τ	100	200	400	800	1600	3200	2 terms	3 terms
0.001	17.94540	17.87125	17.85256	17.84788	17.84671	17.84642	17.84632	17.84632
0.01	5.68924	5.66583	5.65994	5.65846	5.65809	5.65800	5.65797	5.65797
0.1	1.84466	1.83741	1.83558	1.83512	1.83501	1.83498	1.83495	1.83491
0.2	1.34020	1.33519	1.33392	1.33360	1.33353	1.33351	1.33345	1.33334
0.4	0.99844	0.99505	0.99419	0.99398	0.99392	0.99391	0.99372	0.99341
1.0	0.72778	0.72662	0.72633	0.72626	0.72624	0.72624	0.72492	0.72370
2.00225	0.63436	0.63412	0.63406	0.63404	0.63404	–		
4.00201	0.62137	0.62133	0.62133	0.62133	0.62134	Steady state:		0.62132

(b)

	N						Small τ solution	
τ	100	200	400	800	1600	3200	2 terms	3 terms
0.001	17.94088	17.86671	17.84802	17.84334	17.84217	17.84188	17.84178	17.84178
0.01	5.67494	5.65148	5.64557	5.64409	5.64372	5.64363	5.64360	5.64360
0.1	1.79936	1.79194	1.79008	1.78961	1.78949	1.78946	1.78952	1.78946
0.2	1.27601	1.27077	1.26945	1.26912	1.26904	1.26902	1.26919	1.26902
0.4	0.90727	0.90356	0.90263	0.90240	0.90234	0.90233	0.90285	0.90234
1.0	0.58089	0.57939	0.57901	0.57892	0.57889	0.57889	0.58125	0.57925
2.00225	0.42388	0.42357	0.42350	0.42350	0.42357	–		
4.00201	0.40523	0.40527	0.40529	0.40529	0.40531	Steady state:		0.40529

the non-dimensional fluid velocity and temperature functions, the large η conditions $f'_{\infty}(\eta) \to 1$ and $\theta(\eta) \to 0$ as $\eta \to \infty$ are satisfied to nine decimal places for $\eta \geqslant 9$.

The first time increment $\Delta\tau_0$ was assigned the value $\Delta\tau_0 = 10^{-10}$ and the adopted time step doubling procedure was successful in increasing this time step to $\Delta\tau = 1.31072 \times 10^{-5}$ at the non-dimensional time $\tau_n^* = 1.24998$, namely the time of termination of the forward integrating procedure. Any smaller time increment was immediately increased by the time step doubling procedure, so that both the subsequent time increments and the numerical solution at corresponding instances were almost unchanged in comparison to those obtained with $\Delta\tau_0 = 10^{-10}$. The numerical value of $\eta_{\infty} = 2\zeta_{\infty}\tilde{\tau}_n^{1/2}$ was calculated to be $\eta_{\infty} = 11.99981$, based upon the actual time $\tilde{\tau}_n = 0.56248$ at which the transfer from the step-by-step method in ζ, τ variables to that in η, τ variables took place.

The value of the tolerance ϵ, as an average error between approximations to the solution of the system H_k^1 over the unknown spatial grid points, was taken to be $\epsilon = 10^{-14}$, with a more restrictive convergence criterion on the solution of the associated nonlinear system of algebraic equations producing almost identical results, any difference certainly being indistinguishable graphically. This observation follows from the fact that the iterative solution of the system H_k^1, associated with the forward integrating procedures, rapidly approaches a limiting value and satisfies the convergence criterion after only a few iterations.

The most significant source of variation in the solutions for the non-dimensional fluid velocity function $(\partial f/\partial\eta)(\eta,\tau) = (\partial F/\partial\zeta)(\zeta(\eta,\tau),\tau)$ and the fluid temperature function $g(\eta,\tau) = G(\zeta(\eta,\tau),\tau)$ arise by considering changes in the number of grid spaces N^{ζ} and N^{η} associated with the step-by-step method in ζ, τ and η, τ variables, respectively. Table 2 illustrates the effect of refining the spatial grid from $N = N^{\zeta} = N^{\eta} = 100$ to 3200 grid spaces, corresponding to reducing $h^{\zeta} = (2/3)h^{\eta} = 0.08$ to $h^{\zeta} = (2/3)h^{\eta} = 0.0025$, by repeatedly doubling the value of N. Comparisons of the predicted values of the non-dimensional skin friction coefficient $C_f \mathrm{Re}_x^{1/2}$ and the local Nusselt number $\mathrm{Nu}/\mathrm{Re}_x^{1/2}$ are presented in Tables 2(a) and (b), respectively, for each value of N, together with the 2- and 3-term small time solution (24), at various times τ for the case of $\mathrm{Pr} = 1$ and $m = 1/5$. It is observed in these cases that, as N increases, the initial development of the numerical solution approaches that of the appropriate small time solution. Table 2 also includes results from the matching numerical procedure, for which the value of $\eta_{\infty} \approx 12$ is maintained, a value which has been shown to be both valid for $\tau \leqslant \tau_n^*$ and as $\tau \to \infty$. The restriction to a finite temporal domain requires that the final, steady-state profiles must be enforced at the finite value $\tau = \tau_{\infty}$, corresponding to $\tau \to \infty$. The solutions for the non-dimensional skin friction coefficient and the local Nusselt number have

been observed to smoothly approach their steady-state solutions when τ_∞ is imposed at $\tau_\infty = 5$, for $\mathrm{Pr} = 1$ and $m = 1/5$, with no significant improvement in accuracy when τ_∞ is extended beyond this value. Each result from the matching solution shown in Table 2 is determined from the solution at the time of termination $\tau_n^* = 1.24998$ of the forward integrating approach to τ_∞ by using 992 temporal grid increments, corresponding to a time step of approximately 0.00378, and thus only the spatial grid was modified to be in accordance with that used in the forward integrating approach. An investigation of the effect of the spatial and temporal grid sizes within the matching procedure on the solutions for the non-dimensional fluid velocity and temperature profiles was performed. For the coarser spatial grids presented in Table 2, the same accuracy can be achieved with fewer temporal grid increments. For the finest spatial grids, computational limitations make the investigation of finer temporal grids a very time consuming process, and the use of more than 992 temporal grid increments for a spatial grid of $N = 1600$ is believed to provide results which will be graphically indistinguishable from those achieved with such a discretisation. The convergence of the iterative scheme is described by the approach of the average absolute error over the solution domain to a specified error tolerance. Due to the slow convergence of this numerical procedure, the error tolerance is made small, namely 5×10^{-10}, and the solutions produced by more restrictive tolerances are graphically indistinguishable from those presented here.

For the example of $\mathrm{Pr} = 1$ and $m = 1/5$ shown in Table 2, the time at which the third term in the small time solution (24) begins to become influential and the time at which the small time solutions become invalid approximately coincide at around $\tau = 0.2$ to 0.4. The influence of the parameters Pr and m on the range of validity of the small time solution will be discussed later. Furthermore, Table 2 demonstrates that, at later times in the transient process, the differences in the results obtained using the different spatial grids are less significant. The solutions achieved using all of these grids are almost graphically indistinguishable at any time value through the transient process. The solutions are all seen to smoothly approach the predicted steady-state values of the non-dimensional skin friction coefficient and the local Nusselt number, almost attaining these values at $\tau \approx 4$. Note that the matching solution was not calculated for $n = 3200$ as it was computationally very expensive. Also, the solution for $n = 1600$ displays a slight maximum value in the local Nusselt number (but no turning point in the non-dimensional skin friction coefficient) which is not significantly noticeable in the coarser grids, and it is for this reason that the steady-state value of the Nusselt number is approached from below on this finer grid, although only to the fifth decimal place.

The slight improvement in the accuracy which is achieved as N increases from $N = 1600$ to 3200 is not justified by the additional computational time required. The efficiency of this numerical procedure enables solutions to be achieved relatively rapidly using $h^\zeta = \frac{2}{3}h^\eta = 0.005$, and, therefore, this value has been used for all of the remaining results presented in this paper, so that $N = 1600$.

Figs. 5(a) and 6(a) show the variation of the non-dimensional fluid velocity $(\partial f/\partial\eta)(\eta,\tau)$ and the non-dimensional fluid temperature $g(\eta,\tau)$ profiles, respectively, at various times τ through the transient process, calculated for $\mathrm{Pr} = 1$ and $m = 1/5$. The final, steady-state profiles, as predicted by Eqs. (25)–(27), are also included in this figure. We see that these profiles evolve monotonically, at least to graphical accuracy, from $\tau = 0$ towards the large time, steady-state solution, although initially the effects due to the change in the surface temperature of the impulsively started surface are not felt near the outer edge of the thermal and velocity boundary layers.

Figs. 7 and 8 show the evolution of the non-dimensional skin friction coefficient $C_f \mathrm{Re}_x^{1/2} = (\partial^2 f/\partial\eta^2)(0,\tau)$ and the local Nusselt number $\mathrm{Nu}/\mathrm{Re}_x^{1/2} = -(\partial g/\partial\eta)(0,\tau)$, respectively, for the case of $\mathrm{Pr} = 1$ and $m = 1/5$, together with the final, steady-state values of these quantities, namely those presented in Table 3(a). The numerical, transient solutions are shown in Figs. 7(a) and 8(a) to develop closely following the small time solution (24), and both the 2- and 3-term solutions are almost graphically identical to the numerical solutions for $\tau \lesssim 1.15$, as is expected from the results presented in Table 2. The 1-term, small time solutions provide an accurate approximation to the numerical solutions only over a relatively limited initial time interval. As the numerical solution begins to deviate from the small time, analytical solution, the truncated series approximations become invalid. The transient development of the non-dimensional skin friction coefficient and the local Nusselt number determined using the matching method, continuing from the forward integrating solution, have been included in Figs. 7 and 8, respectively. In addition, Figs. 7(b) and 8(b) display the approach of the transient, numerical solutions towards the corresponding large time, steady-state value predicted in Table 3(a). For the case of $\mathrm{Pr} = 1$ and $m = 1/5$, the solutions for the non-dimensional skin friction coefficient and the local Nusselt number approximately reach their steady-state values at $\tau \approx 2.5$, from a graphical viewpoint. The 3-term small time solutions are again included in Figs. 7(b) and 8(b) to further demonstrate the ranges over which the initial and final asymptotic solutions can be applied. It should be noted that Figs. 7(b) and 8(b) have been presented using a logarithmic horizontal axis to enable the solutions discussed in Section 6.2 to be directly compared.

Finally, in order to be applicable to practical engineering problems, we have developed a simple matching solution for the non-dimensional skin friction coefficient and compared this with the full numerical solution. Although these matching solutions are not unique, it is sometimes convenient, for engineering purposes, to seek a closed form approximate solution which may be used with confidence over the whole time interval range of interest. Such approximations are used in preference to performing a complete numerical solution of the problem. The simplest example of such a matching solution uses the 3-term small time solution during the majority of the transient regime, which has been shown to provide an accurate initial approximation, and the

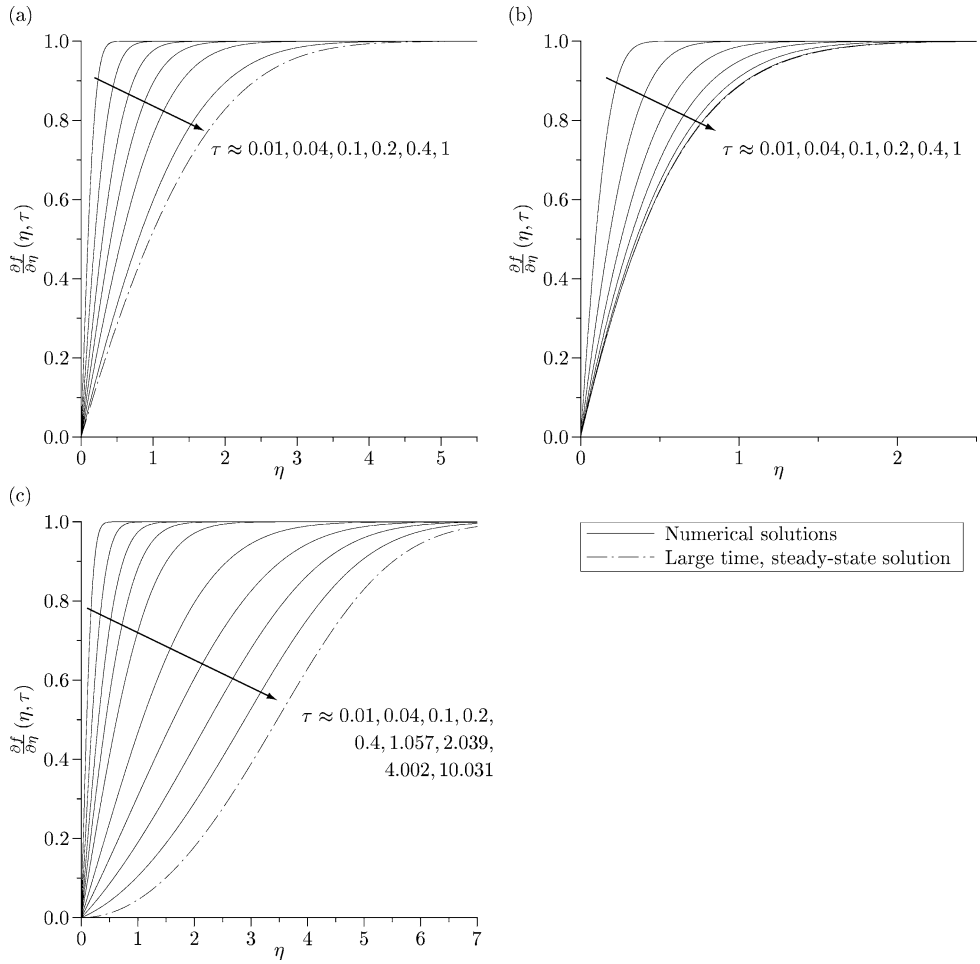

Fig. 5. The profiles of the non-dimensional fluid velocity $(\partial f/\partial \eta)(\eta, \tau)$ at different values of the non-dimensional time τ for (a) $m = 1/5$, (b) $m = 2$, and (c) $m = m^*$.

constant, large time, steady-state values at later times. The transfer between the two parts of the approximate solution occurs at the time $\tau_{\rm tr}$, which is defined to be the first time at which the two functions are equal. Thus, this approximate solution has the following form:

$$\tau_{\rm tr} = \begin{cases} \dfrac{1}{\sqrt{\pi}}\tau^{-\frac{1}{2}} + \dfrac{m}{\sqrt{\pi}}\left(1 + \dfrac{4}{3\pi}\right)\tau^{\frac{1}{2}} + \dfrac{1}{2}F_2''(0)\tau^{\frac{3}{2}} & \text{for } \tau \leqslant \tau_{\rm tr}, \\ f_\infty''(0) & \text{for } \tau \geqslant \tau_{\rm tr}, \end{cases} \tag{51}$$

where $\tau_{\rm tr}$ is the smallest time ($\tau_{\rm tr} > 0$) at which

$$\frac{1}{\sqrt{\pi}}\tau_{\rm tr}^{-1/2} + \frac{m}{\sqrt{\pi}}\left(1 + \frac{4}{3\pi}\right)\tau_{\rm tr}^{1/2} + \frac{1}{2}F_2''(0)\tau_{\rm tr}^{3/2} = f_2''(0). \tag{52}$$

The accuracy of such an approximation is immediately evident from Fig. 7(b), where each of the two parts of the solution are displayed for a range of values of m. It is clear that there is always a period of time over which the 3-term small time solution has become invalid but the large time, steady-state solution has not been reached. To rectify this inaccuracy, we consider a matching function of the following form:

$$C_f {\rm Re}_x^{1/2} = \frac{1}{\sqrt{\pi\tau}}\left[\pi\left(f_\infty''(0)\right)^2\tau + \exp\left(-\alpha\tau - \gamma\tau^2\right)\right]^{\frac{1}{2}}, \tag{53}$$

which, by construction, has the correct behaviour as $\tau \to \infty$ and matches the leading-order term in the small time solution (24), provided that $\alpha > 0$ and $\gamma > 0$. To derive appropriate values for α and γ, a Maclaurin series expansion, valid for small values

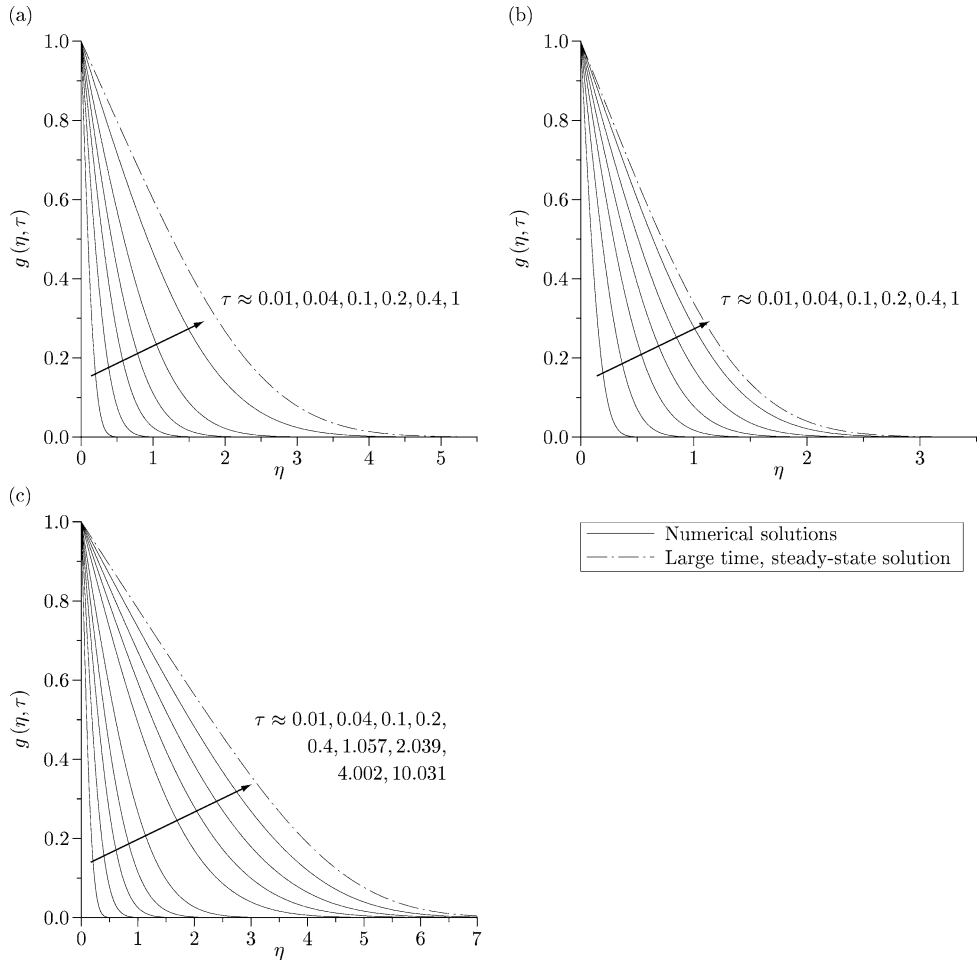

Fig. 6. The profiles of the non-dimensional fluid temperature $g(\eta,\tau)$ at different values of the non-dimensional time τ for (a) $m = 1/5$, (b) $m = 2$, and (c) $m = m^*$, when $\mathrm{Pr} = 1$.

of τ, was used to obtain agreement with the coefficients of the 3-term form of the small time solution (24). Based upon this procedure, the values of α and γ are chosen according to

$$\alpha = \pi\left(f''_\infty(0)\right)^2 - 2m\left(1+\frac{4}{3\pi}\right),$$
$$\gamma = -\sqrt{\pi}F''_2(0) + \frac{1}{2}\pi^2\left(f''_\infty(0)\right)^4 - 2m\pi\left(1+\frac{4}{3\pi}\right)\left(f''_\infty(0)\right)^2 + m^2\left(1+\frac{4}{3\pi}\right)^2. \tag{54}$$

For $m = 1/3$, the comparison provided in Figs. 7(a) and 7(b) between the empirical formula (53), where $\alpha = 0.8528$ and $\gamma = 0.1768$, and the full numerical solution demonstrates that this matching solution can be used with confidence over the whole range of values of τ to within 1% relative error, and may therefore be used with confidence in engineering applications. For clarity, solutions for other values of m have not been presented. The empirical formula (53) breaks down for $\tau > 4$ when $m = m^*$, although this non-physical case is of less engineering significance. For other values of m considered, the empirical formula (53) was shown to provide an excellent matching solution, namely to within 1% relative error in comparison to the full numerical solution.

6.2. *Solutions for other values of* Pr *and* m

As Pr and m were varied from $\mathrm{Pr} = 1$ and $m = 1/5$, the only parameters within the numerical procedures which were found to be necessary to change from those discussed in Section 6.1, i.e., those parameters which produced any significant change in

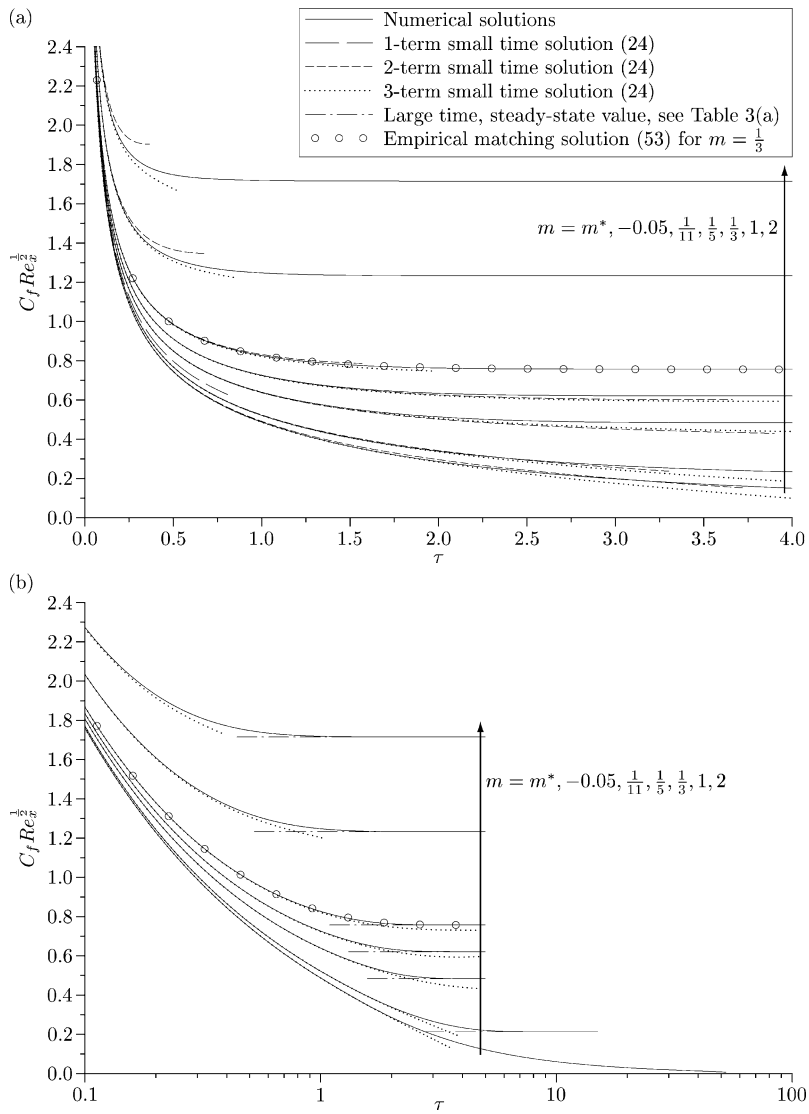

Fig. 7. Evolution of the non-dimensional skin friction coefficient $C_f \mathrm{Re}_x^{1/2} = (\partial^2 f/\partial\eta^2)(0,\tau)$ for different values of m in comparison with (a) the small time solution (24), using 1, 2, and 3 terms, and (b) the 3-term small time solution together with the predicted large time, steady-state value, see Table 3(a), presented with a logarithmic horizontal τ axis. The empirical approximation (53) is presented only for the case of $m = 1/3$.

the solutions presented within the figures contained in this paper, were the values of η_∞ and τ_∞. The values stated below are sufficiently large for any further increase to produce results which are graphically indistinguishable from those presented in the figures. These increases in the values of η_∞ and τ_∞, which specify corresponding values of the independent variable which are considered to be equivalent to infinity when applying boundary conditions, reflect increases in the thermal and velocity boundary-layer thicknesses and the time required to reach a steady-state solution, as appropriate.

For $\mathrm{Pr} = 1$, further numerical solutions were determined for the cases of $m = m^*$, -0.05, $1/11$, $1/3$, 1, and 2, with necessary increases in η_∞ for $m = m^*$ and -0.05 to $\eta_\infty = 15$, resulting in a necessary increase in N to $N = 2000$, thereby maintaining the same value of the spatial grid increment for the step-by-step solution procedures. In addition, the value of τ_∞ had to be increased for the chosen values of $m < 0$ and the matching numerical procedure exhibited a significant increase in computational time required to satisfy the convergence criterion. Accordingly, for $m = -0.05$, the value $\tau_\infty = 15$ and a temporal grid of 400 time steps was used to produce the results presented in the figures. For $m = m^*$, the results presented here have been based upon $\tau_\infty = 57$ and 800 temporal grid increments, a calculation which required a significant amount of computational time, namely of the order of 430 hours on a 1.5 GHz Pentium 4 PC workstation. In the case of $m = m^*$, this value of τ_∞ is not

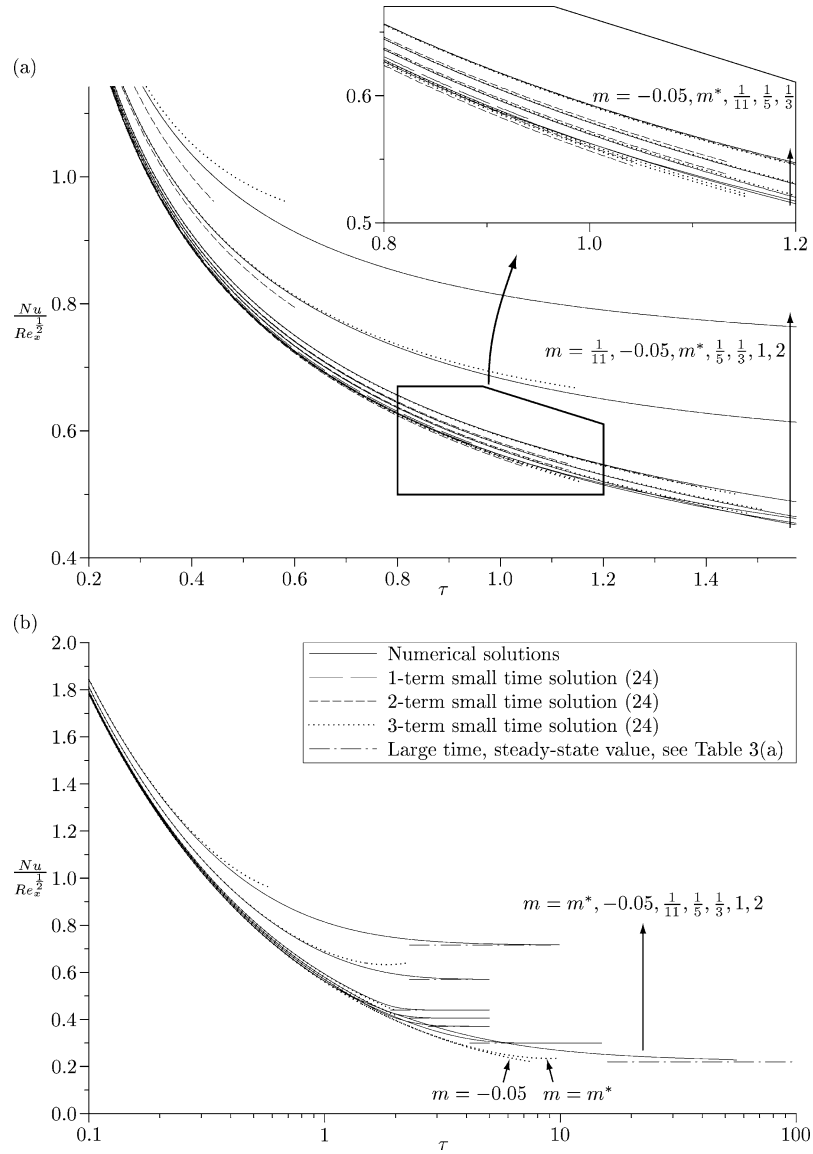

Fig. 8. Evolution of the local Nusselt number $\mathrm{Nu}/\mathrm{Re}_x^{1/2} = -(\partial g/\partial \eta)(0, \tau)$ for different values of m when $\mathrm{Pr} = 1$ in comparison with (a) the small time solution (24), using 1, 2, and 3 terms, and (b) the 3-term small time solution together with the predicted large time, steady-state value, see Table 3(a), presented with a logarithmic horizontal τ axis.

believed to represent that value beyond which a negligible effect on the numerical solution is observed and does not lead to a completely smooth approach to the predicted steady-state values of the appropriate quantities. In fact the value of τ_∞ which would be required to guarantee this, whilst maintaining a sufficiently small temporal grid increment, is beyond our computational limitations. For the remaining values of $m < 1$, the value of $\tau_\infty = 5$, as used in Section 6.1, was maintained, and only the number of temporal grid increments were modified according to the value of $\tau_n^* \approx 1/(1-m)$, whilst maintaining the same time step value as used for $\mathrm{Pr} = 1$ and $m = 1/5$. It should also be noted that, although the matching numerical procedure is not required and so a value of τ_∞ is not imposed, the time at which the steady-state solution is reached has increased for $m = 2$ in comparison to $m = 1$.

As described in Section 6.1 for $\mathrm{Pr} = 1$ and $m = 1/5$, the corresponding numerical and asymptotic solutions for the non-dimensional skin friction coefficient and the local Nusselt number are presented in Figs. 7 and 8, respectively, for the cases of $m = m^*$, -0.05, $1/11$, $1/3$, 1, and 2, when $\mathrm{Pr} = 1$. As for the case of $m = 1/5$, the range of validity of the 1-term, small time solution (24) is significantly improved when either 2 or 3 terms are used in this approximation. As m increases above

Table 3
The predicted steady-state values of the non-dimensional skin friction coefficient $C_f \mathrm{Re}_x^{1/2} = f''_\infty(0)$ and the local Nusselt number $\mathrm{Nu}/\mathrm{Re}_x^{1/2} = -g'_\infty(0)$, which are valid for large values of τ, for (a) different values of m when the Prandtl number $\mathrm{Pr} = 1$, and (b) different values of the Prandtl number Pr when $m = 1/5$

(a)

		m					
	m^*	-0.05	$1/11$	$1/5$	$1/3$	1	2
$f''_\infty(0)$	0.0	0.2134837	0.4837449	0.6213238	0.7574476	1.2325877	1.7150680
$-g'_\infty(0)$	0.2197199	0.2994299	0.3707422	0.4052868	0.4400745	0.5704653	0.7160707

(b)

	Pr				
	0.72	1	2	5	10
$-g'(0)$	0.3583393	0.4052868	0.5224002	0.7239136	0.9220919

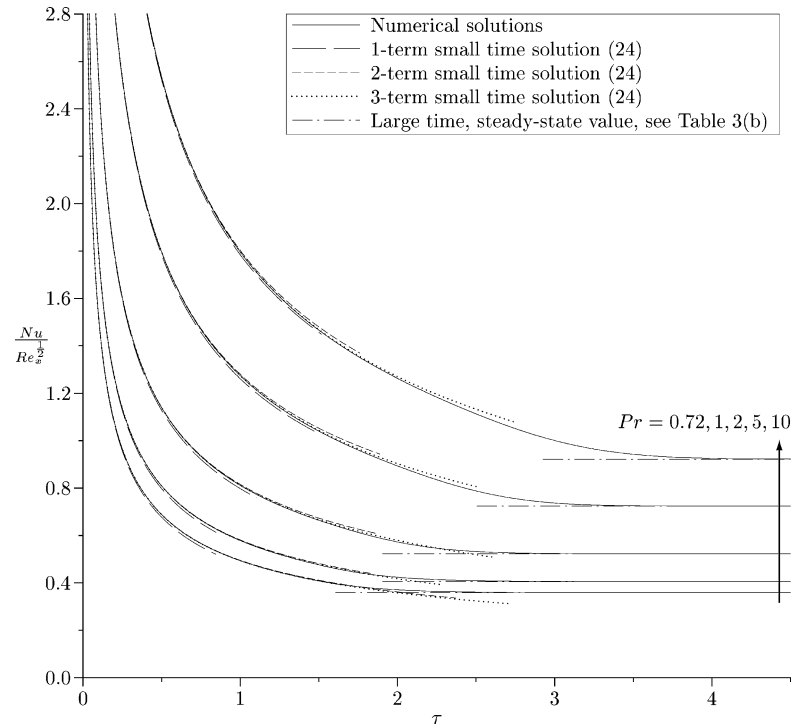

Fig. 9. Evolution of the local Nusselt number $\mathrm{Nu}/\mathrm{Re}_x^{1/2} = -(\partial g/\partial \eta)(0,\tau)$ for different values of the Prandtl number Pr when $m = 1/5$ in comparison with the small time solution (24), using 1, 2, and 3 terms, and the predicted large time, steady-state value, see Table 3(b).

$m = 1/5$, the range over which the corresponding small time solutions are indistinguishable from the numerical solutions decreases, although the inclusion of the third term has an increasingly more significant influence on the approximation. For $m^* \leqslant m \leqslant 1/5$, these 3-term solutions are all valid until between $\tau \approx 1.0$ and 1.15, but this upper limit is significantly reduced to $\tau \approx 0.15$ for $m = 2$. As described above, for the case of $m = m^*$, the value of τ_∞ could not be taken sufficiently large for the steady-state solutions for the non-dimensional skin friction coefficient and the local Nusselt number to be approached smoothly. Based upon some smaller values of τ_∞, the displayed portions of these numerical solutions are believed to be accurate. For all other values of m, the large time, steady-state values presented in Table 3 are approached smoothly.

The evolutions of the non-dimensional fluid velocity and temperature profiles for the extreme cases of $m = m^*$ and $m = 2$, when $\mathrm{Pr} = 1$, are presented in Figs. 5, (b) and (c), and 6, (b) and (c). The profiles for $m = 2$ are similar in nature to those for $m = 1/5$, being plotted at the same time instants as those for $m = 1/5$. The clear difference is the expected reduction in the

thermal and velocity boundary-layer thicknesses as m is increased from $m = 1/5$ to 2. The corresponding solution profiles for $m = m^*$ are significantly different in nature and reflect both the increased thermal and velocity boundary-layer thickness, and the large increase in the time taken to reach the steady-state conditions. The solution profiles for other values of m between these extremes represent an obvious progression through the three cases presented in each of Figs. 5 and 6.

In order to demonstrate the influence of the Prandtl number on the solution of this problem, the evolution of the local Nusselt number has been presented in Fig. 9 for $\mathrm{Pr} = 0.72$, 1, 2, 5, and 10, when $m = 1/5$. For each value of Pr, the local Nusselt number is presented in comparison to the 1-, 2-, and 3-term small time solutions (24) and the large time solution presented in Table 3(b). In general, the inclusion of the second term in the small time solution (24) for the local Nusselt number is observed to extend significantly the upper range of validity of this approximation. The additional inclusion of the third term is, as expected from the values for $G_2'(0)$ in Table 1(b), more effective in further extending this upper τ limit as Pr increases over the range $\mathrm{Pr} = 0.72$ to 10. As Pr increases, so does the time τ taken to reach the steady-state solution for the local Nusselt number, and the small time approximations break down at an increasingly smaller proportion of the total transient time. The equivalent profiles to those shown in Figs. 5 and 6 for $\mathrm{Pr} \neq 1$ are similar in nature and, therefore, have not been presented here.

7. Conclusions

The present paper is concerned with the momentum and thermal, laminar boundary layers resulting from an impulsive Falkner–Skan problem, where appropriate physical cases relate to the flow past an impulsively started, sharp, semi-infinite wedge. The external inviscid flow is given by $u_e(x) = x^m$, for $m < 1$. The forced convection, thermal boundary-layer is produced by the sudden increase of the surface temperature as the motion is started. The initial development of these boundary layers has satisfactorily been represented by a series solution for small times. The solution for large time approaches steady state and is given by the Falkner–Skan equation, which includes, as special cases, the famous Blasius solution, when $m = 0$, and the Hiemenz stagnation point flow, when $m = 1$, see Rosenhead [30]. Precise details in the transition range between small (initial, unsteady state) and large (final, steady-state) times were obtained using a very accurate numerical method. This method consists of a modification of the forward integration procedure proposed by Merkin [18] in combination with a finite-difference method similar to that devised by Dennis [19], applied beyond times at which the initial marching procedure is no longer well posed, and the results have been validated against the small time solution. It has been shown that the small time transient is initially confined within a region close to the surface, but, as time progresses, diffusion effects eventually modify the solution at a great distance from the surface. Also, in the approach to the large time, the deviation from the steady-state velocity and temperature profiles is concentrated near to the surface. Further, we have shown that our solutions include all of the previously known solutions as special cases. In addition, for the steady state, new solutions are found for $m > 1$ and for different values of the Prandtl number Pr. However, it should be mentioned that the value $\beta = 2$ ($m \to \infty$) corresponds to the instantly accelerating flow. Physically, this extreme case does not really exist since, as the wedge angle increases to 2π ($\beta \to 2$), the space for the fluid shrinks to zero. The effect of the Prandtl number on the heat transfer rate has been also investigated for the representative case of a wedge angle of 60°, i.e., $m = 1/5$. As expected, an increase in the value of Pr, which occurs in the governing equation (10) as the coefficient $1/\mathrm{Pr}$ of the thermal diffusion term, results in an increase in the time taken to reach the steady-state solution (see Fig. 9) and a decrease in the thermal boundary-layer thickness (see Fig. 4). We notice that the present large time solution for the heat transfer characteristics are in very good agreement with all of the previously reported results, see, for example, Lin and Lin [25].

The Falkner–Skan one-parameter family of solutions of the boundary-layer equations has proved to be very useful in the interpretation of fluid flows at large Reynolds numbers. For steady Falkner–Skan flows, various properties of this family of solutions have been discussed extensively in the literature for all relevant values of the exponent m, see Section 4 and the references cited therein. Although the analysis of the unsteady momentum equation has been developed to some extent by Stewartson, Nanbu and Smith, fundamental aspects of transient heat transfer still remain to be described. Over recent years, problems involving unsteady conditions of motion and heating of bodies in fluids have become increasingly important in engineering applications such as aerodynamics and hydrodynamics, for example, the flow created by the passage of a shock wave over a surface. The problem considered in this paper has practical value in the understanding of the transient development of such systems.

The very accurate numerical techniques employed in Harris et al. [20,21,23] have been applied to the problem considered by Watkins [14] and the results demonstrate that these finite-difference techniques provide great advantages in the computation of the unsteady momentum and thermal boundary layers for transient Falkner–Skan flows. A comparison of the results of Watkins [14] with those presented here shows very good agreement for all of the common solution parameters. Another advantage of the technique used in this paper is the reduction of the number of independent variables from three to two by an appropriate scaling, while Watkins [14] has used the second order, zig–zag, finite-difference scheme devised by Krause.

Finally, it is worth mentioning that, in spite of the extensive studies of the steady-state flows past wedges of various configurations, there is still a need for accurate solution methods for fluids of any Prandtl number. The techniques employed in this paper could be applied to the study of more complicated situations by removing some of the restrictions, such as constant properties or the absence of viscous dissipation. The present solution method can also be applied to other wedge, forced convection, heat transfer problems, especially for uniform flux cases. We hope to report solutions for this case in a forthcoming paper.

Acknowledgements

All of the authors would like to thank the referees for their very constructive comments on the first draft of this paper. Further, two of the authors, D.B. Ingham and I. Pop, gratefully acknowledge some financial support from The Royal Society.

References

[1] L.G. Leal, Laminar Flow and Convection Transfer Processes: Scaling Principles and Asymptotic Analysis, Butterworth-Heinemann, Boston, 1992.
[2] K. Gersten, H. Herwig, Strämungsmechanik, Vieweg, Braunschweig/Wiesbaden, 1992.
[3] H. Schlichting, K. Gersten, Grenzschicht – Theorie, Springer-Verlag, Berlin, 1997.
[4] N. Riley, Unsteady laminar boundary layers, SIAM Rev. 17 (1975) 274–297.
[5] N. Riley, Unsteady viscous flows, Sci. Progress Oxford 74 (1990) 361–377.
[6] D.R. Telionis, Review – unsteady boundary-layers, separated and attached, J. Fluids Engrg. 101 (1979) 29–43.
[7] D.R. Telionis, Unsteady Viscous Flows, Springer-Verlag, New York, 1981.
[8] D.K. Ludlow, P.A. Clarkson, A.P. Bassom, New similarity solutions of the unsteady incompressible boundary-layer equations, Quart. J. Mech. Appl. Math. 53 (2000) 175–206.
[9] I. Pop, F. Arinç, Transient heat transfer in boundary-layer flows, in: J. Padet, F. Arinç (Eds.), Proc. Int. Symposium on Transient Convective Heat Transfer, Cesme, Turkey, 19–23 August, Begell House, New York, 1996, pp. 3–17.
[10] J.D.A. Walker, S.C.R. Dennis, The boundary-layer in a shock tube, J. Fluid Mech. 56 (1972) 19–47.
[11] S.H. Smith, The impulsive motion of a wedge in a viscous fluid, J. Appl. Math. Phys. (ZAMP) 18 (1967) 508–522.
[12] K. Nanbu, Unsteady Falkner–Skan flow, J. Appl. Math. Phys. (ZAMP) 22 (1971) 1167–1172.
[13] M.G. Hall, The boundary-layer over an impulsively started flat plate, Proc. R. Soc. London A 310 (1969) 401–414.
[14] C.B. Watkins, Unsteady heat transfer in impulsive Falkner–Skan flows, Int. J. Heat Mass Transfer 19 (1976) 395–403.
[15] E.H. Krause, T. Bothmann, Numerische Stabilität Dreidimensionaler Grenzschtlosungen, J. Appl. Math. Mech. (ZAMM) 48 (1968) 1336–1342.
[16] J.C. Williams, T.B. Rhyne, Boundary-layer development on a wedge impulsively set into motion, SIAM J. Appl. Math. 38 (1980) 215–224.
[17] S.-Y. Tsay, Y.-P. Shih, Laminar forced convection in wedge flow with separation, J. Chinese Inst. Engrs. 2 (1979) 53–57.
[18] J.H. Merkin, Free convection with blowing and suction, Int. J. Heat Mass Transfer 15 (1972) 989–999.
[19] S.C.R. Dennis, The motion of a viscous fluid past an impulsively started semi-infinite flat plate, J. Inst. Math. Appl. 10 (1972) 105–117.
[20] S.D. Harris, L. Elliott, D.B. Ingham, I. Pop, Transient free convection flow past a vertical flat plate subjected to a sudden change in surface temperature, Int. J. Heat Mass Transfer 41 (1998) 357–372.
[21] S.D. Harris, D.B. Ingham, I. Pop, Free convection from a vertical plate in a porous medium subjected to a sudden change in surface heat flux, Transp. Porous Media 26 (1997) 207–226.
[22] S.D. Harris, D.B. Ingham, I. Pop, Free convection from a vertical plate in a porous media subjected to a sudden change in surface temperature, Int. Comm. Heat Mass Transfer 24 (1997) 543–552.
[23] S.D. Harris, D.B. Ingham, I. Pop, Unsteady mixed convection boundary-layer flow on a vertical surface in a porous medium, Int. J. Heat Mass Transfer 42 (1999) 357–372.
[24] S.D. Harris, D.B. Ingham, I. Pop, Transient boundary-layer heat transfer from a flat plate subjected to a sudden change in heat flux, Eur. J. Mech. B/Fluids 20 (2001) 187–204.
[25] H.-T. Lin, L.-K. Lin, Similarity solutions for laminar forced convection heat transfer from wedges to fluids of any Prandtl number, Int. J. Heat Mass Transfer 30 (1987) 1111–1118.
[26] R.S. Heeg, D. Dijkstra, P.J. Zandbergen, The stability of Falkner–Skan flows with several inflection points, Z. Angew. Math. Phys. (ZAMP) 50 (1999) 82–93.
[27] K. Stewartson, Further solutions of the Falkner–Skan equation, Proc. Cambridge Philos. Soc. 50 (1954) 454–465.
[28] D.R. Hartree, On an equation occurring in Falkner and Skan's approximate treatment of the equations of the boundary-layer, Proc. Cambridge Philos. Soc. 33 (1937) 223–239.
[29] W.H.H. Banks, P.G. Drazin, Perturbation methods in boundary-layer theory, J. Fluid Mech. 58 (1973) 763–775.
[30] L. Rosenhead, Laminar Boundary Layers, Oxford University Press, 1963.